Cell Reports
Medicine

Article

Microbiota-produced immune regulatory bile acid metabolites control central nervous system autoimmunity

Graphical abstract

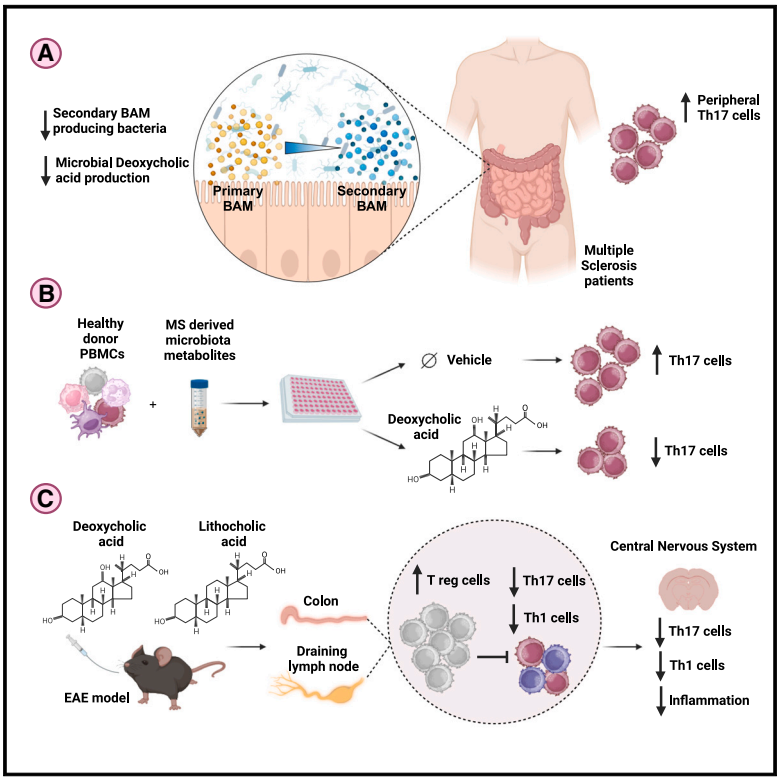

Highlights

- Bacteria releasing bile acid metabolites are decreased in the gut of MS patients
- Reduction of bile acid metabolite DCA is associated with high Th17 cells in MS
- Immune regulatory bile acid metabolites prevent central nervous system autoimmunity

Authors

Martina Antonini Cencicchio, Federico Montini, Vittoria Palmieri, ..., Vittorio Martinelli, Roberto Furlan, Marika Falcone

Correspondence

falcone.marika@hsr.it

In brief

Antonini Cencicchio et al. reveal that gut microbiota-related deficiency of deoxycholic acid (DCA), an immune regulatory bile acid metabolite, is present in MS patients and linked to increased peripheral Th17 cell frequency. The beneficial role of immune regulatory BAM in central nervous system autoimmunity was validated in a preclinical model of MS.

Antonini Cencicchio et al., 2025, Cell Reports Medicine 6, 102028
April 15, 2025
https://doi.org/10.1016/j.xcrm.2025.102028

CellPress

Cell Reports Medicine

CellPress
OPEN ACCESS

Article

Microbiota-produced immune regulatory bile acid metabolites control central nervous system autoimmunity

Martina Antonini Cencicchio,[1] Federico Montini,[1,2] Vittoria Palmieri,[1] Luca Massimino,[3,4] Marta Lo Conte,[1] Annamaria Finardi,[5] Alessandra Mandelli,[5] Francesco Asnicar,[6] Radmila Pavlovic,[7] Denise Drago,[7] Federica Ungaro,[3,4] Annapaola Andolfo,[7] Nicola Segata,[6] Vittorio Martinelli,[2] Roberto Furlan,[5] and Marika Falcone[1,8,*]

[1]Autoimmune Pathogenesis Unit, IRCCS San Raffaele Scientific Institute, 20132 Milan Italy
[2]Clinical Neurology Unit, IRCCS Ospedale San Raffaele, 20132 Milan, Italy
[3]Experimental Gastroenterology Unit, IRCCS San Raffaele Scientific Institute, 20132 Milan, Italy
[4]Gastroenterology and Digestive Endoscopy Department, IRCCS Ospedale San Raffaele, 20132 Milan, Italy
[5]Clinical Neuroimmunology Unit, INSPE, IRCCS San Raffaele Scientific Institute, 20132 Milan, Italy
[6]Department CIBIO, University of Trento, 38123 Trento, Italy
[7]Proteomics and Metabolomics Facility (ProMeFa), IRCCS San Raffaele Scientific Institute, 20132 Milan, Italy
[8]Lead contact
*Correspondence: falcone.marika@hsr.it
https://doi.org/10.1016/j.xcrm.2025.102028

SUMMARY

The commensal gut microbiota has a role in the pathogenesis of extra-intestinal autoimmune diseases such as multiple sclerosis (MS) with unknown mechanisms. Deoxycholic acid (DCA) and lithocholic acid (LCA) are secondary bile acid metabolites (BAMs) produced from primary bile acids by gut microbiota that play key immune regulatory functions by promoting FOXP3^{+} regulatory T (Treg) cell differentiation at the expense of Th17 cells. Here, we show that bacteria releasing enzymes responsible for secondary BAMs production are under-represented in the gut of MS patients, resulting in significantly reduced intestinal concentration of DCA and immune dysregulation with increased percentage of Th17 cells. We validated our human findings in a preclinical model of MS by showing that DCA/LCA administration prevents experimental autoimmune encephalomyelitis (EAE) by dampening Th17 cell differentiation and the effector phenotype of myelin-reactive T cells. Our data highlight the key role of immune regulatory BAMs for the prevention of central nervous system (CNS) autoimmunity.

INTRODUCTION

Multiple sclerosis (MS) is a chronic inflammatory disease of the CNS caused by the autoimmune-mediated destruction of the myelin sheath with consequent loss of neurological functions and progressive disability.[1] The gut environment is instrumental in regulating CNS autoimmunity in humans and preclinical models of MS.[2–5] In support of this view, alterations of the commensal gut microbiota are found in MS patients and are associated with immune dysregulation, i.e., increased percentages of effector Th17 cells, and with high disease activity.[5,6] The mechanisms through which the commensal gut microbiota regulate CNS autoimmunity in MS are largely unknown. The current hypothesis holds that gut bacteria regulate CNS autoimmunity by modulating activation and acquisition of an effector Th17 cell phenotype by dormant myelin-reactive T cells.[7] Metabolites released or modified by the gut microbiota play key immune regulatory function and could modulate MS pathogenesis by affecting the functional phenotype of myelin-specific autoreactive T cells. The protective role of tolerogenic microbiota-produced metabolites such as short-chain fatty acids (SCFAs) and indole metabolites (tryptophan derivatives) has been demonstrated in humans[8,9] and preclinical models of MS.[10,11] Secondary bile acid metabolites (BAMs) and, specifically, deoxycholic acid (DCA), lithocholic acid (LCA), and their derivatives, represent a newly characterized group of microbial metabolites[12] whose immune regulatory function and capacity to dampen effector T cell responses in CNS autoimmunity were poorly investigated.

Bile acids (BAs) are key digestive molecules whose primary function is to enable fat emulsification for the absorption of fatty acids and liposoluble molecules within the intestine. Recent evidence indicates that BAs play additional key roles that regulate energy expenditure, lipid and glucose metabolism, and the immune system.[13,14] Primary BAs conjugated with taurine and glycine groups are post-prandially released into the duodenum, and most of them are reabsorbed in the terminal ileum to circulate back to the liver. Primary BAs that are not reabsorbed at the ileal level (about 5%–10%) are unconjugated by bile salt hydrolase (BSH) enzymes and enter the large intestine becoming

substrate for further bacterial-mediated transformation. Different intestinal bacterial taxa from common genera such as *Bacteroides*, *Eubacterium*, and *Clostridium* release BSH that allows the deconjugation of taurine- and glycine-conjugated BAs.[15] At colonic level, unconjugated BAs are further modified by enteric commensals through different metabolic pathways, including oxidation, epimerization, esterification, desulfation, and 7-α-dehydroxylation.[16,17] In particular, the 7-α-dehydroxylation is the enzymatic reaction that produces DCA and LCA that, together with their derivatives, play important immune regulatory functions being able to drive intestinal differentiation of FOXP3$^+$ regulatory T (Treg) cells at the expenses of effector Th17 and Th1 cells.[18–20] DCA/LCA and their derivatives exert their immune regulatory properties by directly interacting with T cells or indirectly through the modulation of the functional phenotype of dendritic cells (DCs) and macrophages. For example, LCA inhibits Th1 cell differentiation by binding the nuclear vitamin D receptor on T cells[21] and an LCA derivative, the 3-oxo-LCA, dampens Th17 cell differentiation by directly binding to the transcription factor RAR-related orphan receptor-γ (ROR-γt).[18] DCA is capable to decrease Th1 and Th17 cell differentiation and their cytokine production by binding the G protein-coupled bile acid receptor 1 (GPBAR1) expressed on DCs.[19] Additionally, isoDCA, a DCA isomer, induces immune tolerance by binding to the farnesoid X receptor (FXR) on DCs thus reducing their immunostimulatory properties and rendering them capable of driving FOXP3$^+$ Treg cell differentiation.[22] DCA/LCA also modulate the functional phenotype of macrophages from a pro-inflammatory M1 toward an anti-inflammatory M2 phenotype thus dampening intestinal inflammation. Such polarization is mediated by the activation of the GPBAR1 receptor and promotes the production of high level of tolerogenic interleukin (IL)-10 and the differentiation of FOXp3$^+$ Treg cells.[23] The immune regulatory properties of DCA/LCA have been clearly demonstrated in different models of colitis in which they dampen intestinal inflammation by inhibiting the release of inflammatory cytokines both in humans with inflammatory bowel disease (IBD)[24] and in preclinical models.[25] Conversely, elevation of DCA and LCA in colon cancer promotes recruitment of intra-tumoral immunosuppressive FOXP3$^+$ Treg cells and cancer growth.[26] So far, the capacity of immune regulatory BAMs such as DCA and LCA and their derivatives to prevent autoimmunity at sites distal from the intestine such as the CNS has been scarcely investigated.

Here, we show that subjects affected by relapsing-remitting (RR) MS (RRMS) have significantly reduced relative abundance of commensal bacterial strains that release enzymes responsible for the biosynthesis of secondary BAMs leading to significantly lower concentration of intestinal DCA. In RRMS subjects, the defective microbiota-regulated biliary network and low intestinal DCA concentration are associated with immune dysregulation and, specifically, with increased relative percentage of circulating effector Th17 cells in the peripheral blood. We validated the key role of the immune regulatory BAMs in controlling CNS autoimmunity by showing that administration of DCA/LCA ameliorates experimental autoimmune encephalomyelitis (EAE), the preclinical model of MS, both at clinical and at histopathological level. We show that DCA/LCA exert their protective effect by promoting FOXP3$^+$ Treg cell expansion and dampening effector Th17 cells in the intestine but also in peripheral lymphoid organs and in the CNS thus reducing the percentage of myelin-specific autoreactive T cells with an effector phenotype.

RESULTS

Low abundance of commensal BAM-producing bacteria in RRMS patients

Several lines of evidence linked dysbiosis with immune dysregulation[6] and disease severity in MS.[5,6] Although those findings suggest a causal role for the gut microbiota in MS pathogenesis, the mechanism through which it impinges on immune dysregulation and CNS autoimmunity remains elusive. We studied the commensal gut microbiota of MS patients in comparison with healthy controls (HCs) by shotgun metagenomic sequencing and extrapolated biochemical pathways associated with known bacterial species based on the Kyoto Encyclopedia of Genes and Genomics (KEGG) database focusing our search on BAM-producing bacteria. In parallel, we performed a metabolomic analysis on fecal samples and immunological profiling on peripheral blood mononuclear cells (PBMCs) in the two cohorts (Figure 1A). The MS population enrolled in our study was highly heterogeneous for clinical signs and symptoms, but all patients were affected by the RR form of the disease (RRMS) with disease duration ranging from 2 to 27 years and different disability scores measured using the Kurtzke expanded disability scale (EDSS) ranging from 0 to 6.5 (Table S1). The HCs were matched for age and BMI with our RRMS patients (Table S2). Our fecal metagenomic data showed no difference in the alpha diversity between RRMS patients and HCs (Figure 1B). However, we found highly significant differences at the species level with 1,886 bacterial taxa differentially represented in the intestine of RRMS patients vs. HCs (Figure 1C and Table S3). Next, we analyzed the intestinal representation of BAM-producing bacteria in RRMS patients and HCs. To this aim, we search by manual annotation the KEGG database for bacterial strains having the necessary enzymes to convert primary BAs into secondary BAMs. Our functional analysis of the gut microbiome revealed that the overall frequency of sequences of bacteria that release enzymes involved in secondary BAMs production, either in primary BA deconjugation (BSH) or directly on their modification into secondary BAMs, was highly significantly reduced in RRMS patients compared to HCs (p = 7.31e−06) (Figure 1D). Notably, RRMS patients showed less relative abundance of some BAM-producing bacterial species such as *Bifidobacterium longum*, *Bifidobacterium pseudocatenulatum*, and *Christensenella minuta* (Figures 1E and S1A) whose immune regulatory function and capacity to dampen inflammation were previously demonstrated both in the intestine[27,28] and in extra-intestinal tissue.[29,30]

Next, to test whether the reduced relative abundance of BAM-producing species resulted in decreased levels of secondary BAMs, we performed metabolomic profiling on stools of RRMS patients and HCs focusing on the biliary network. Our metabolomic analysis by ultra-performance liquid chromatography/mass spectrometry (UPLC/MS) revealed no differences in the fecal concentration of primary BAs such as cholic acid, glycocholic acid, taurocholic acid, chenodeoxycholic acid, and

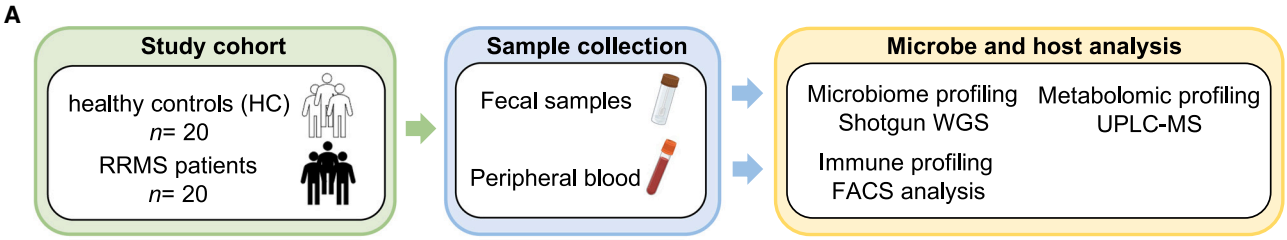

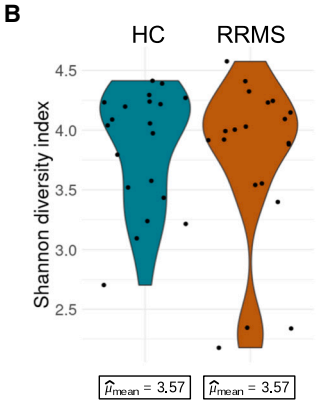

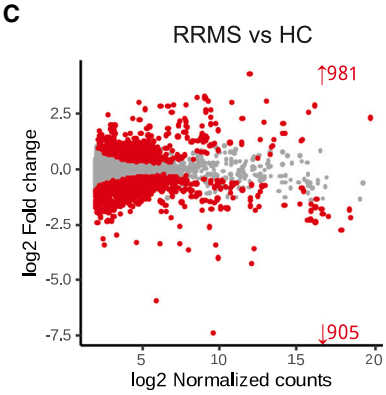

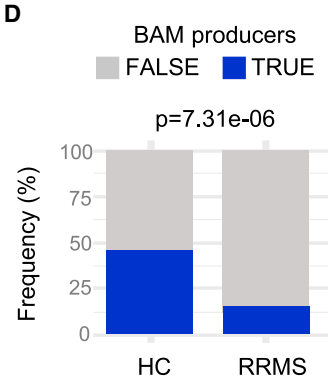

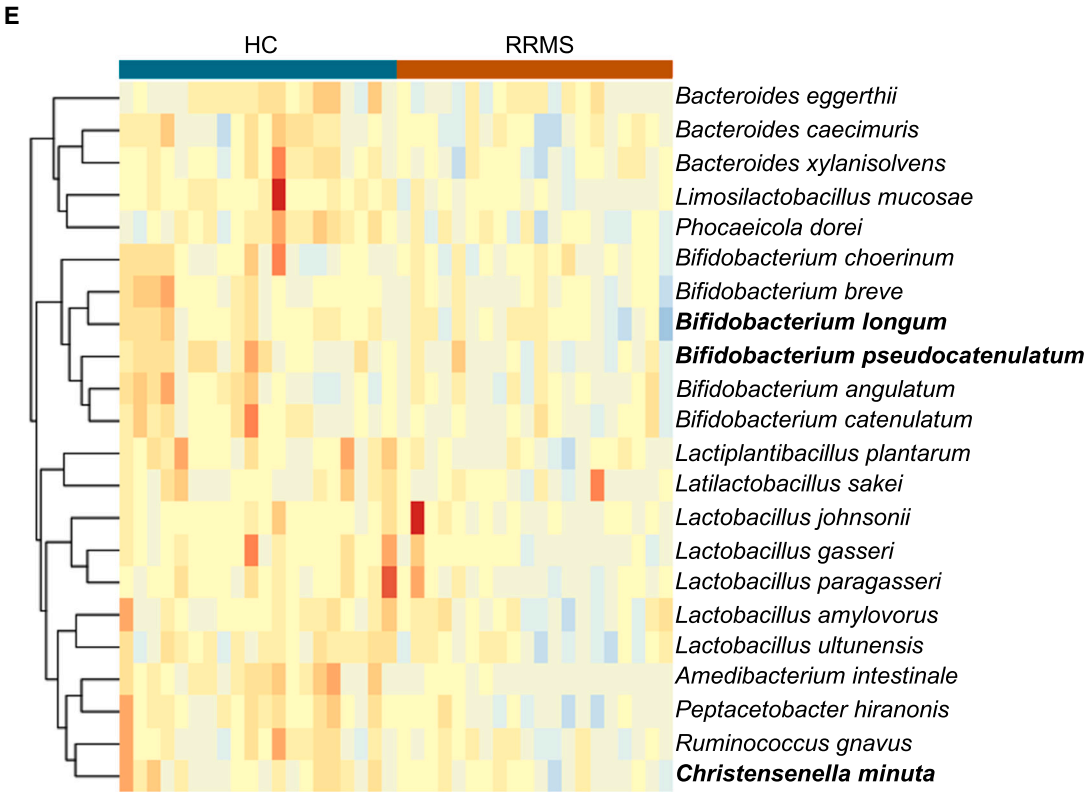

Figure 1. Reduced representation of BAM-producing bacteria in the gut microbiome of RRMS patients

(A) Schematic representation of the human study.

(B) Violin plots showing alpha diversity in HCs (n = 20) and RRMS patients (n = 20) based on Shannon index.

(legend continued on next page)

glycochenodeoxycholic acid between the two cohorts (Figure S2), thus suggesting a normal capacity of hepatocytes to release primary BAs in RRMS patients. Conversely, when we looked at the concentrations of secondary BAMs, we detected a highly significant reduction of the immune regulatory DCA in RRMS patients compared to HCs ($p < 0.0001$) (Figure 2A). Intestinal levels of other secondary BAMs like glycodeoxycholic acid, taurodeoxycholic acid, LCA, taurolithocholic acid, glycoursodeoxycholic acid, and taurohyodeoxycholic acid, were unaltered in our RRMS cohort compared to HCs (Figure 2A). We performed a multivariate analysis to exclude possible confounding factors that could have altered DCA concentration in RRMS patients such as sex, age, neurological disability (i.e., EDSS score), disease duration, and hepatic function (hepatic enzymes: aspartate transaminase (AST), alanine transaminase (ALT), gamma-glutamyl transferase (GGT), and bilirubin levels). Our analysis demonstrated that the intestinal concentration of DCA was exclusively dependent on the occurrence of RRMS condition and was not affected by age, sex, hepatic function, disability, or disease duration (Figure 2B).

Having found a specific reduction of intestinal DCA in RRMS patients, we asked whether bacterial species that release enzymes involved in the multistep pathway of 7-α-dehydroxylation that is crucial to produce DCA were under-represented in the intestine of our RRMS cohort. We found that several bacteria releasing enzymes involved in 7-α-dehydroxylation and DCA production such as *Clostridium hylemoneae*, *Bifidobacterium pseudocatenulatum*, *Paeniclostridium sordellii*, *Paraclostridium bifermentans*, and *Clostridium hiranonis* were significantly reduced in RRMS fecal samples compared to HCs (Figures 2C and S1B).[30–33]

The microbiota-induced metabolic profile and, specifically, secondary BAMs, are important to control immune homeostasis in the intestine and systemically. Hence, we asked whether altered metabolic profile and low DCA concentration lead to immune dysregulation in RRMS patients. Our multiparametric fluorescence-activated cell sorting (FACS) analysis on PBMCs highlighted a significant increase in the percentage of circulating effector Th17 cells in RRMS patients compared to HCs (Figure 3A). On the contrary, the percentage of circulating mucosa-associated invariant T (MAIT) cells, a T cell subset linked with intestinal homeostasis and tissue regeneration,[34] were reduced in RRMS patients (Figure 3A) in accordance with previous findings.[35] The percentages of other T cell subsets including Th1, Th2, $\gamma\delta$ T cells, and FOXP3$^+$ Treg cells were not altered in PBMCs of RRMS patients (Figure 3A). We performed a correlative analysis to link percentage of Th17 cells in PBMCs and intestinal DCA concentration. The analysis revealed an inversed correlation although not statistically significant (Figure S3A), possibly due to the fact that Th17 cell percentage in the PBMCs only partially reflects intestinal Th17 cell percentage. We also did not find a correlation between Th17 cell percentages and disease severity (EDSS score) in RRMS patients (Figure S3B). Furthermore, the RRMS patients of our cohort who showed clinical and/or neuroradiological disease activity in a 12 months follow-up (2 out of 20, see Table S1) did not have particularly high Th17 cell percentages (red dots in Figure 3A). The latter findings suggest that increase in Th17 cells in RRMS patients is not related to clinical signs of disease. To further link the expansion of Th17 cells in RRMS to the gut microbiota profile, we tested the capacity of RRMS fecal filtrates (containing no live bacteria but microbial components including metabolites)[36] to induce human naive T cells (from HC PBMCs) toward an Th17 cell phenotype. Figure 3B shows that the gut microbiota from RRMS patients favored differentiation of Th17 cells, supporting the notion that the microbial/metabolic contents in the intestine of RRMS patients promote Th17 cell differentiation. Importantly, adding exogenous DCA to the RRMS microbiota-PBMC co-cultures reduced Th17 cell differentiation (Figure 3C). Those findings validated the importance of the functional profile of the gut microbiota for the increased Th17 cell differentiation that we found in the PBMCs of RRMS patients. The effect was specific for the Th17 cell subset, and other T lymphocyte populations such as Th1 cells and FOXP3$^+$ Treg cells were not differentially induced by RRMS vs. HC gut microbial products (Figure 3B).

Immune regulatory BAMs reduce CNS autoimmunity

In order to validate the immune regulatory role of secondary BAMs in CNS autoimmunity, we increased intestinal concentrations of DCA/LCA in the intestine of mice affected by EAE, the preclinical model of RRMS, and tested the effect on disease occurrence. Previous studies showed that supplementation with DCA and LCA ameliorates gut inflammation in different animal models of colitis.[25] Hence, we orally administered an emulsion of DCA and LCA to C57BL/6 mice to create a tolerogenic BAM-enriched gut environment and tested the immune regulatory effect on CNS autoimmunity. First, we demonstrated that, under basal conditions, i.e., in the absence of inflammation in naive not-EAE-immunized mice, increasing intestinal concentration of DCA/LCA promotes FOXP3$^+$ Treg cell differentiation (Figure S4). Next, to test the effect of DCA/LCA supplementation on the occurrence of CNS autoimmunity, we orally administered DCA/LCA to EAE mice daily starting one week before immunization and continuing up to three weeks after EAE induction (Figure 4A). EAE was induced by subcutaneous immunization in the back of C57BL/6 mice with the peptide 35-55 of the myelin oligodendrocyte glycoprotein (MOG_{35-55} peptide) emulsified in complete Freund's adjuvant (CFA) with the addition of pertussis toxin. This immunization procedure induces a strong effector MOG-specific T cell response in the inguinal and axillary draining lymph nodes (DLNs) from where activated MOG-specific T cells travel to the CNS to mediate myelin destruction.[37] Remarkably, we found attenuated signs of EAE in BAM-treated mice with

(C) MA plot showing the differential abundance of bacterial species significantly altered in HCs and RRMS patients (false discovery rate [FDR] < 0.1).
(D) Frequency of reads related to BAM-producing bacteria in HCs and RRMS patients.
(E) Heatmap showing the relative abundance of relevant BAM-producer bacterial species that were significantly reduced in RRMS patients (FDR < 0.1).
See also Tables S1 and S2 and Figure S1A.

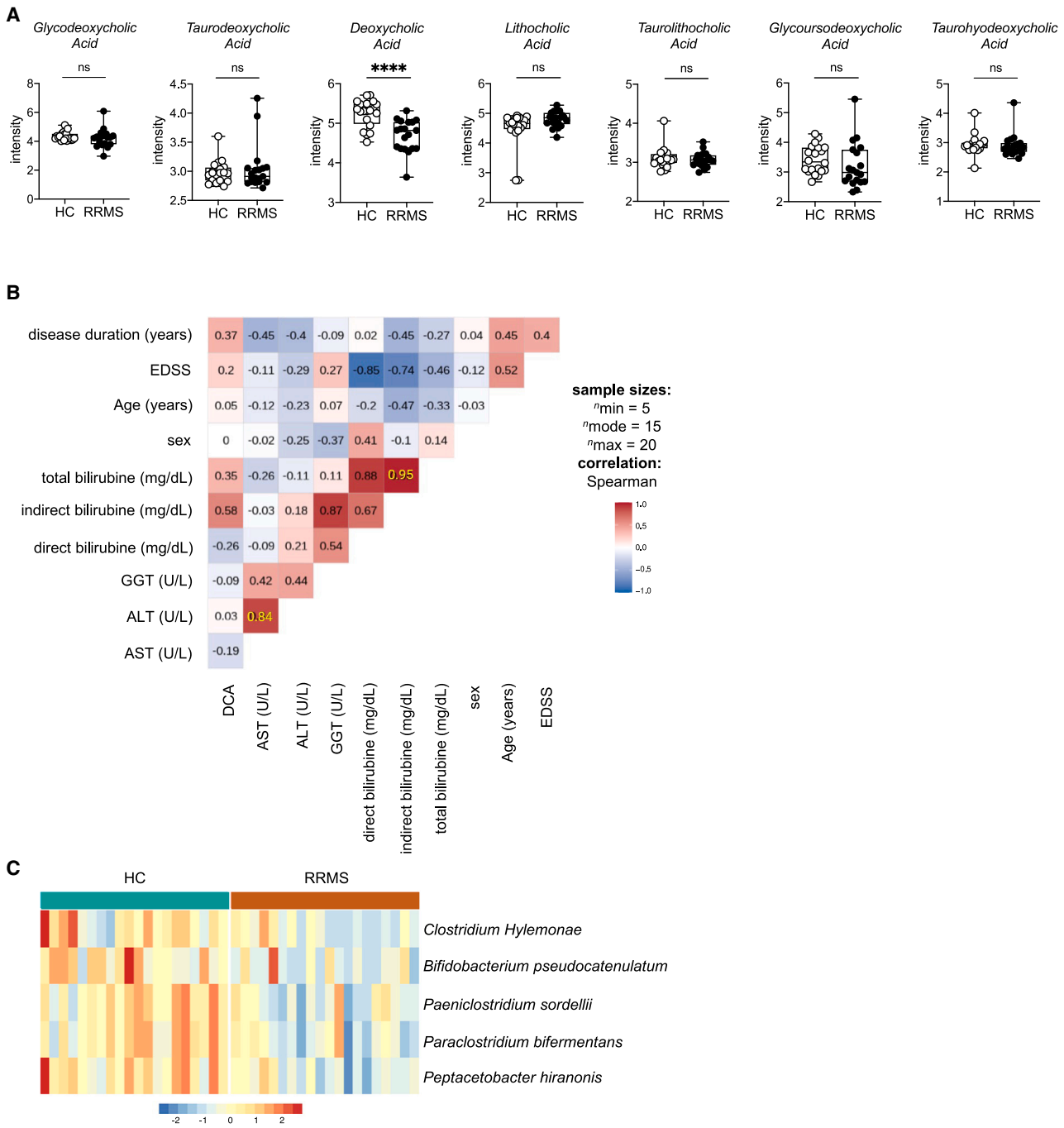

Figure 2. Low DCA concentrations in the intestine of RRMS correlate with disease occurrence

(A) Boxplots of UPLC mass spectrometry peak intensity (logarithmic scale) showing the abundance of secondary BAMs detected in fecal samples of RRMS patients (n = 19) and HCs (n = 20). Data were generated upon Mann-Whitney U test among the two experimental sample groups.

(B) Multivariate analysis showing correlation among the concentration of DCA, hepatic functions (AST, ALT, GGT, direct bilirubin, indirect bilirubin, and total bilirubin), clinical data (disease duration and EDSS), and potential confounders such as age and sex. Multivariate analysis was performed by Spearman correlation coefficients and adjusted by FDR. Correlation coefficients in yellow are significant at $p < 0.05$.

(C) Bacterial species releasing enzymes performing 7-α-dehydroxylation that were significantly reduced in RRMS samples compared to HCs (FDR < 0.1).

*$p < 0.05$; **$p < 0.01$; ***$p < 0.001$; ****$p < 0.0001$; ns, not significant. See also Figures S1B and S2.

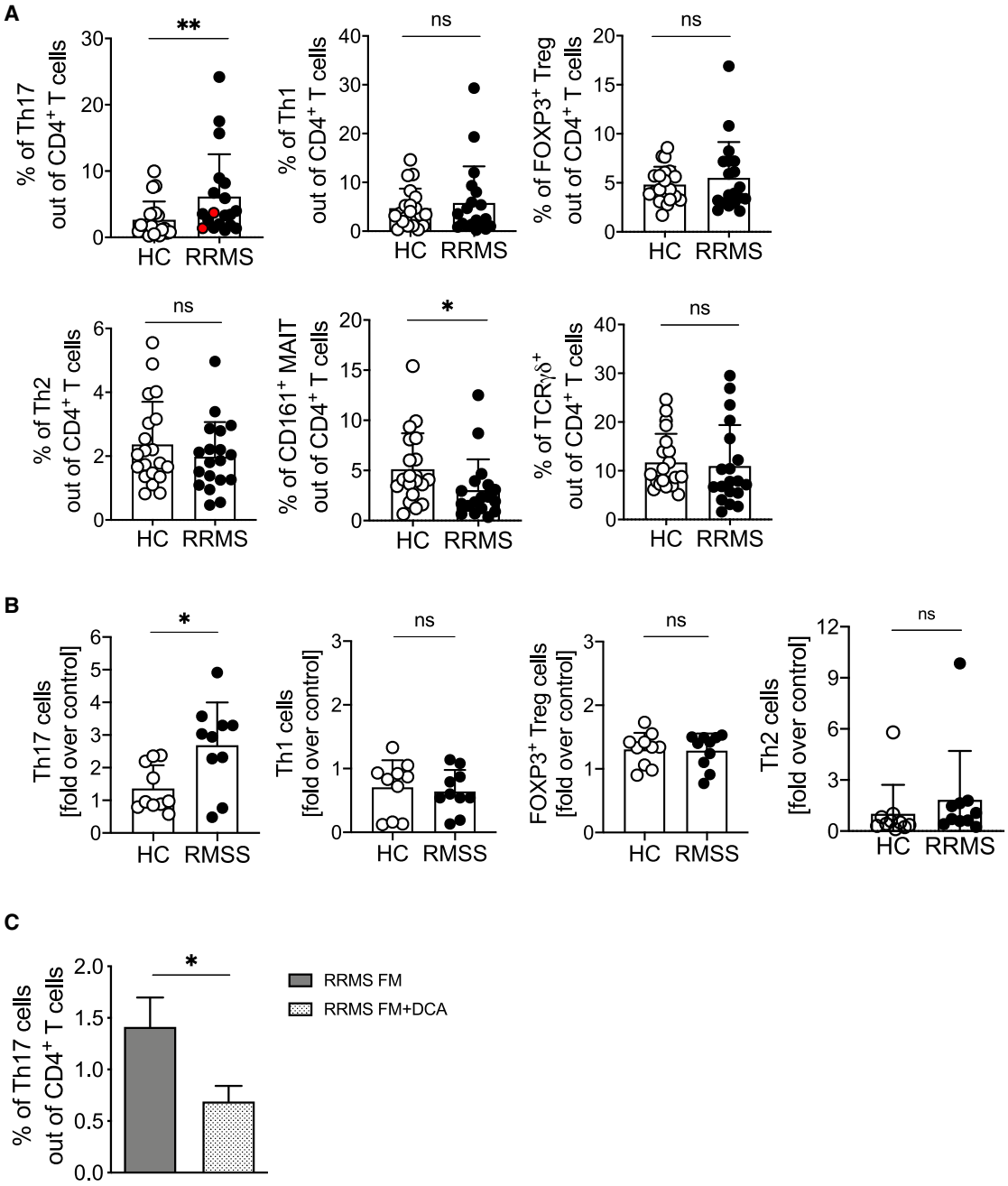

Figure 3. Alteration of the microbiota-regulated metabolic profile is linked to immune dysregulation in RRMS

(A) Percentage of circulating T cell subsets in RRMS patients and HCs measured by multiparametric flow cytometry. γδT cells were identified as CD45$^+$CD3$^+$TCRγδ$^+$ cells; MAIT cells were defined as CD161$^+$TCRVα7.2$^+$ of CD3$^+$TCRγδ$^-$ cells. Among non-MAIT/non-TCRγδ CD4$^+$ T cells, we identified Treg cells as CD25$^+$FOXP3$^+$ cells. Finally, the FOXP3-negative T cell population was further divided in the following effector T helper (Th) cells: Th1 as FOXP3$^-$Tbet$^+$, Th17 as FOXP3$^-$RORγt$^+$, and Th2 as FOXP3$^-$CRTH2$^+$.

(B) *In vitro* expansion of Tbet$^+$ Th1, RORγt$^+$ Th17, FOXP3$^+$ Treg cells and CRTH2$^+$ Th2 cells in response to gut microbial filtrates of HCs and RRMS patients. PBMCs from a healthy donor were cultured for 72 h in the presence of fecal filtrates derived from HCs or RRMS patients and analyzed by flow cytometry as in (A). Each symbol represents a fecal sample donor (n = 10 per group). Data are expressed as fold difference over vehicle control (no fecal filtrates).

(C) Percentage of *in vitro* expanded RORγt$^+$ Th17 cells in response to gut microbial filtrates of RRMS patients supplemented or not with 10 μM DCA. PBMCs from a healthy donor were cultured for 72 h and subsequently analyzed by flow cytometry (n = 10 fecal sample donor per group).

Bars represent the mean ± SD of data from two independent experiments. All statistical analyses were performed using Mann-Whitney U test to compare the RRMS group with the HC group or the RRMS fecal material (FM) group with the RRMS FM + DCA group. *p < 0.05, **p < 0.01; ns, not significant. See also Figures S3 and S8.

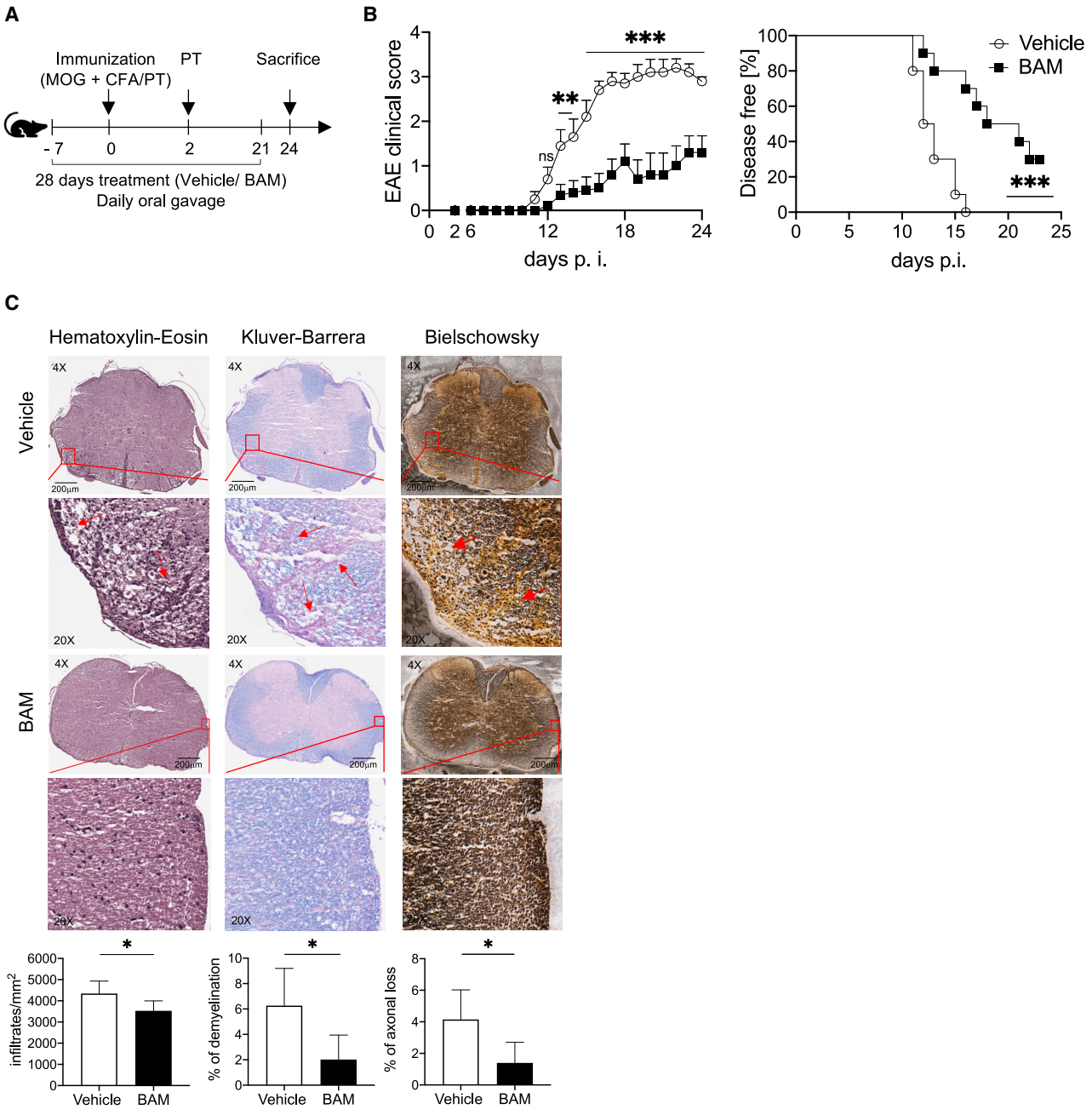

Figure 4. Supplementation with immune regulatory secondary bile acid metabolites (BAM) dampens CNS autoimmunity

(A) Schematic illustration of EAE induction and DCA/LCA supplementation.

(B) Clinical score and disease incidence in MOG_{35-55} immunized mice following BAM supplementation (n = 10 mice per group); clinical score data are expressed as mean ± SEM. EAE clinical scores were analyzed with two-way ANOVA test followed by Bonferroni post-testing for multiple comparisons. Disease incidence was evaluated using the Kaplan-Meier estimation, whereas statistical significance was evaluated by the log rank (Mantel-Cox) test.

(C) Histological analysis of the spinal cord of EAE-immunized mice receiving BAM or vehicle (n = 5 mice per group). Adjacent sections are stained to detect lymphocyte infiltrates (hematoxylin and eosin staining), demyelination (Kluver-Barrera staining), and axonal loss (Bielschowsky staining). Magnification 20×. Scale bar 200 µm.

Bars represent the mean ± SD. Unpaired t test was used for statistical analysis. One representative experiment out of two is shown. *p < 0.05, **p < 0.01, ***p < 0.001; ns, not significant. See also Figures S5 and S6.

significantly reduced clinical scores when compared to their untreated counterparts (Figure 4B). In addition, while 100% of untreated mice developed EAE by day 16 post-EAE immunization (p.i.), a large fraction of BAM-treated mice (35%) were completely protected and showed no sign of disease up to 24 days post-EAE immunization (Figure 4B). Protection from CNS autoimmunity was confirmed at the histopathological level with a significantly lower lymphocyte infiltration associated with reduced demyelination and axonal loss in the CNS of BAM-treated compared to untreated EAE mice (Figure 4C). Since DCA was the immune regulatory BAM selectively reduced in RRMS patients, we asked whether DCA alone was sufficient to induce protection against CNS autoimmunity. We repeated the experiment by administering either DCA/LCA or DCA alone and observed that DCA was sufficient to induce protection from EAE, but with a lower statistical power compared to DCA/LCA, thus suggesting a synergistic effect of the two immune regulatory BAMs (Figure S5). Those results demonstrate that increasing the intestinal levels of immune regulatory BAMs prevents CNS autoimmunity. To test whether immune regulatory BAMs are also capable to suppress ongoing CNS autoimmunity, we administered DCA/LCA 10 days after EAE immunization, when MOG-reactive T cells are already activated and biased toward an effector T cell phenotype. In this setting, we observed only a slight but not significant protection from EAE in BAM-treated mice (Figure S6), arguing that the immune regulatory mechanisms triggered by DCA/LCA are effective in reducing the induction phase of CNS autoimmunity but cannot suppress ongoing myelin-specific effector T cell responses.

Immune regulatory BAMs promote immune tolerance at the intestinal level

Our next goal was to address how immune regulatory BAMs control CNS autoimmunity. Profiling of gut mucosal immunity by FACS analysis confirmed the presence of a pro-inflammatory T cell profile with expansion of effector Th17 cells and reduction of FOXP3$^+$ Treg cells in EAE mice compared to not-EAE-immunized mice (Figure S7). DCA/LCA supplementation significantly increased percentages (Figure 5A) of FOXP3$^+$ Treg cells in the intestine of EAE mice as in steady-state conditions in not-EAE-immunized mice (Figure S4). In addition, in BAM-treated EAE mice, we also detected a significant increase of regulatory Tr1 cells and a significant reduction of effector Th17 and Th1 cells that was not observed in BAM-treated not-EAE-immunized mice (Figure 5A). BAMs administration did not alter the relative percentages of CD4$^+$ T cells, so thatthe increase of regulatory FOXP3$^+$ Treg/Tr1 cells and the decrease of effector Th17/Th1 cells in BAM-treated mice were confirmed also in terms of absolute number of cells (Figure 5B). Those findings suggest that the immune regulatory effect of secondary BAM on dampening Th17/Th1 cell differentiation in the intestine occurs only under inflammatory conditions, possibly to control pathological effector T cell expansion. EAE-immunized mice normally show alterations of the gut environment with damage to the gut barrier integrity and intestinal inflammation.[38] Hence, we asked whether DCA/LCA supplementation modulate the functional phenotype of T cells indirectly by reducing the inflammatory cytokine profile of the gut mucosa. Quantitative RT-PCR of the cytokine profile on the intestinal mucosal tissue revealed gut inflammation with increased expression of *Il6*, *Il1b*, and *Tnfa* encoding genes in EAE-immunized mice at day 7 post-immunization and at the time of EAE occurrence. In BAM-treated mice, the pro-inflammatory cytokine profile was reduced in mice with clinical signs of EAE (Figure 5C) but not at earlier time point (7 days pi, data not shown), suggesting that the reduction of the pro-inflammatory cytokine profile in the intestinal tissue is subsequent and not directly responsible for the Teff→Treg cell shift.

Immune regulatory BAMs suppress differentiation of effector MOG-specific Th17 cells

To test whether BAM-mediated immune regulation extends beyond the intestinal tissue and regulates myelin-specific T cells in extra-intestinal districts, we assessed the functional profiles of T cells isolated from lymph nodes draining the site of EAE immunization (DLNs) and from the CNS (brain and spinal cord). In line with our findings in the intestine, we detected a statistically significant reduction in the relative percentages of effector Th17 cells associated with an increase of regulatory FOXP3$^+$ Treg in the DLNs of BAM-treated EAE mice (Figure 6A). A fraction of regulatory FOXP3$^+$Treg and effector Th17 cells but also Th1 and Tr1 cells present in the DLNs of EAE-immunized mice originated from the gut mucosa as demonstrated by their expression of the gut homing marker $\alpha4\beta7$ (Figure 6B). Notably, BAMs supplementation increased the percentages of FOXP3$^+$ Treg cells of intestinal origin ($\alpha4\beta7^+$FOXP3$^+$ Treg) present in the DLNs (Figure 6B), whereas the frequency of effector $\alpha4\beta7^+$ Th17 and Th1 cells did not change, thus suggesting that the reduced percentage of Th17 cells in the DLNs may be due to a suppressive effect of BAM-induced Treg cells at the site of EAE immunization rather than in the gut. In the CNS of BAM-treated EAE mice, we did not detect an increase in the relative percentage of FOXP3$^+$ Treg cells but a statistically significant reduction of effector Th17 and Th1 cells that particularly regarded GM-CSF$^+$Th1 and GM-CSF$^+$Th17 cells (Figure 6C), T cell subsets with high pathogenic effect in EAE.[39] This finding suggests that a reduced number of myelin-reactive T cells bearing an effector Th17 cell phenotype differentiate in the DLNs from where they reach the CNS. This hypothesis was further supported by our observation of a statistically significant reduction of T cells bearing an effector Th17 and GM-CSF$^+$Th17 phenotype in MOG-stimulated T cell cultures obtained from DLNs of BAM-treated mice compared to untreated counterparts (Figure 6D). Finally, we interrogated the mechanism through which immune regulatory BAMs regulate the Teff/Treg cell ratio among myelin-reactive T cells. Recent lines of evidence demonstrated the capacity of DCA to modulate adaptive immunity and the Teff/Treg ratio by acting on DCs.[19] Hence, we tested whether BAM-modulated DCs pulsed with the MOG_{35-55} peptide antigen modulate the functional phenotype of myelin-reactive T cells (naive MOG_{35-55}-specific T cells isolated from 2D2 TCR^{MOG} transgenic mice). We found that antigen-specific stimulation of naive MOG_{35-55}-specific T cells with DCA-modulated DCs significantly reduced their differentiation toward the effector Th17 and Th1 cell phenotype, also inhibiting the generation of GM-CSF$^+$Th1 and GM-CSF$^+$Th17 cells that have high encephalitogenic potential (Figure 7), thus confirming our *ex vivo* data of

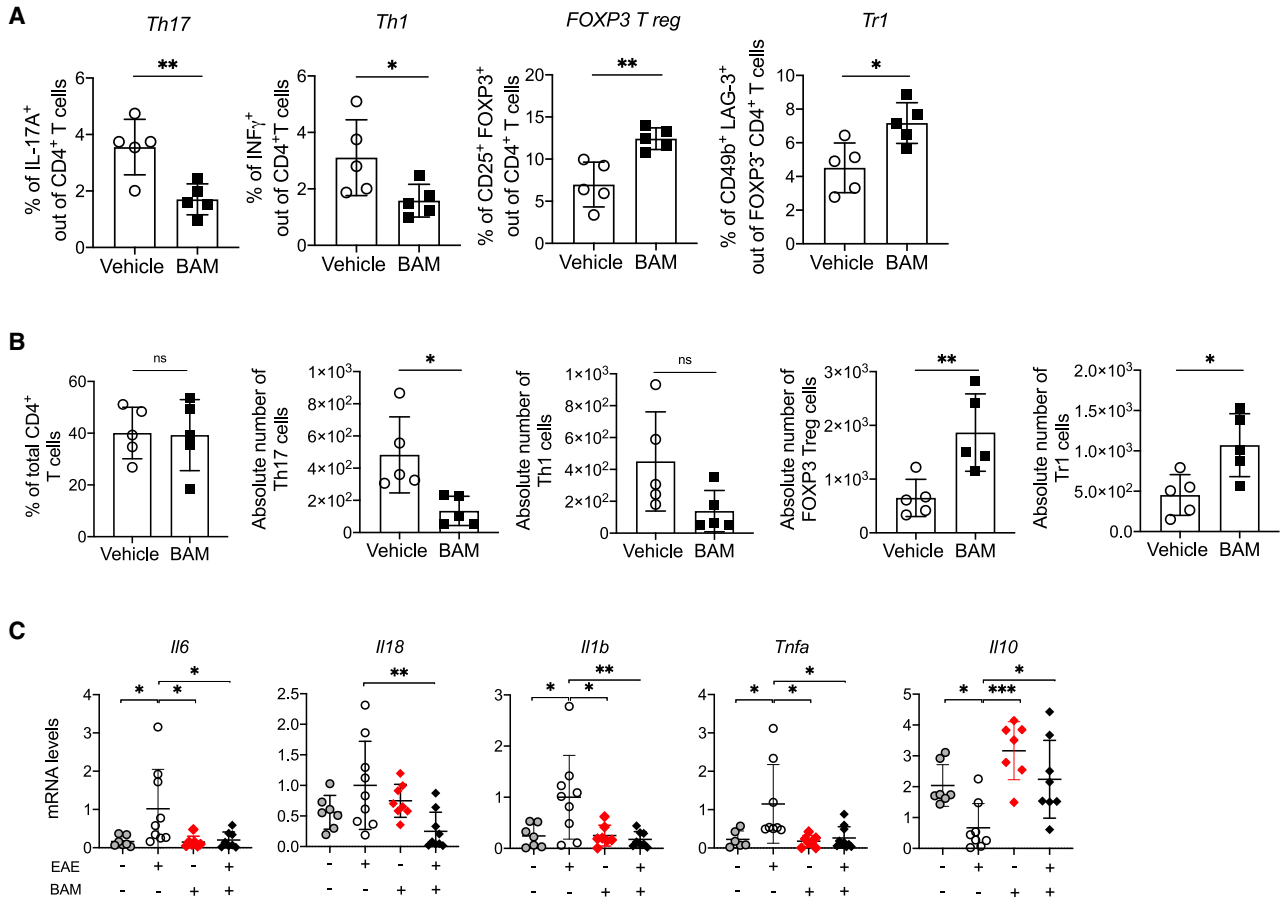

Figure 5. Immune regulatory secondary bile acid metabolites (BAM) reduce inflammation and promote intestinal immune tolerance in EAE mice

(A) Percentages of CD4$^+$ T cells expressing IL-17A (Th17), IFN-γ (Th1), FOXP3 and CD25 (FOXP3$^+$ Treg), or LAG3 and CD49b (FOXP3$^-$ Tr1) in the intestine of EAE mice supplemented with BAM or vehicle (n = 5 mice per group).

(B) percentages of total CD4$^+$ T cells and absolute numbers of effector Th17, Th1, and regulatory FOXP3 and Tr1 cells in the intestinal mucosa of EAE-immunized mice (n = 5 mice per group), treated or not with BAM. Bars represent the mean ± SD. Unpaired t test was used.

(C) RT-qPCR analysis of cytokine mRNA expression in the intestine of EAE-immunized mice at the time of onset of clinical signs of the disease and control (not immunized) mice receiving oral BAM supplementation or vehicle (n = 7–10 mice per group).

Data are expressed as mean ± SD. One-way ANOVA was performed, followed by Tukey's test. Data are from one representative experiment out of two. *$p < 0.05$, **$p < 0.01$, ***$p < 0.001$. ns, not significant. See also Figures S4, S7, and S9.

reduced GM-CSF$^+$Th1 and GM-CSF$^+$Th17 cells in BAM-treated mice (Figure 6C). We demonstrated that LCA was also capable of modulating the functional profile of DCs and of reducing their capacity to trigger MOG-specific effector GM-CSF$^+$Th1 and GM-CSF$^+$Th17 cells (Figure 7). Our data suggest that BAM-modulated DCs within the intestine and/or peripheral lymph nodes dampen the differentiation of myelin-specific effector T cells thus reducing the number of highly pathogenic GM-CSF$^+$Th17/Th1 cells reaching the CNS.

DISCUSSION

The commensal gut microbiota plays a key role in the pathogenesis of MS. Accordingly, numerous studies reported alterations of the commensal gut microbiota in MS patients including a recent study in a large cohort of RRMS subjects that linked the beneficial effect of treatment with specific gut microbiota profiles.[5] It is now clear that the gut microbiota has a complex structure, and it is not the presence of a single bacterial strain to modulate the immune system but rather the whole microbiota-associated metabolic potential assembled at the intestinal level by different combinations of microbial strains. In fact, the metabolic environment created in the intestine by the commensal microbiota either through direct release of microbial metabolites or through modification of food components or endogenous metabolites is fundamental to control host immunity and autoimmunity and to dampen harmful inflammatory responses. So far, in patients and preclinical models of MS, immune regulatory metabolites such as SCFAs[8,11] and the indole metabolites (tryptophan derivatives)[9,10] have been largely investigated while a limited number of studies have been performed on the role of microbiota-produced secondary BAMs in MS pathogenesis.[40]

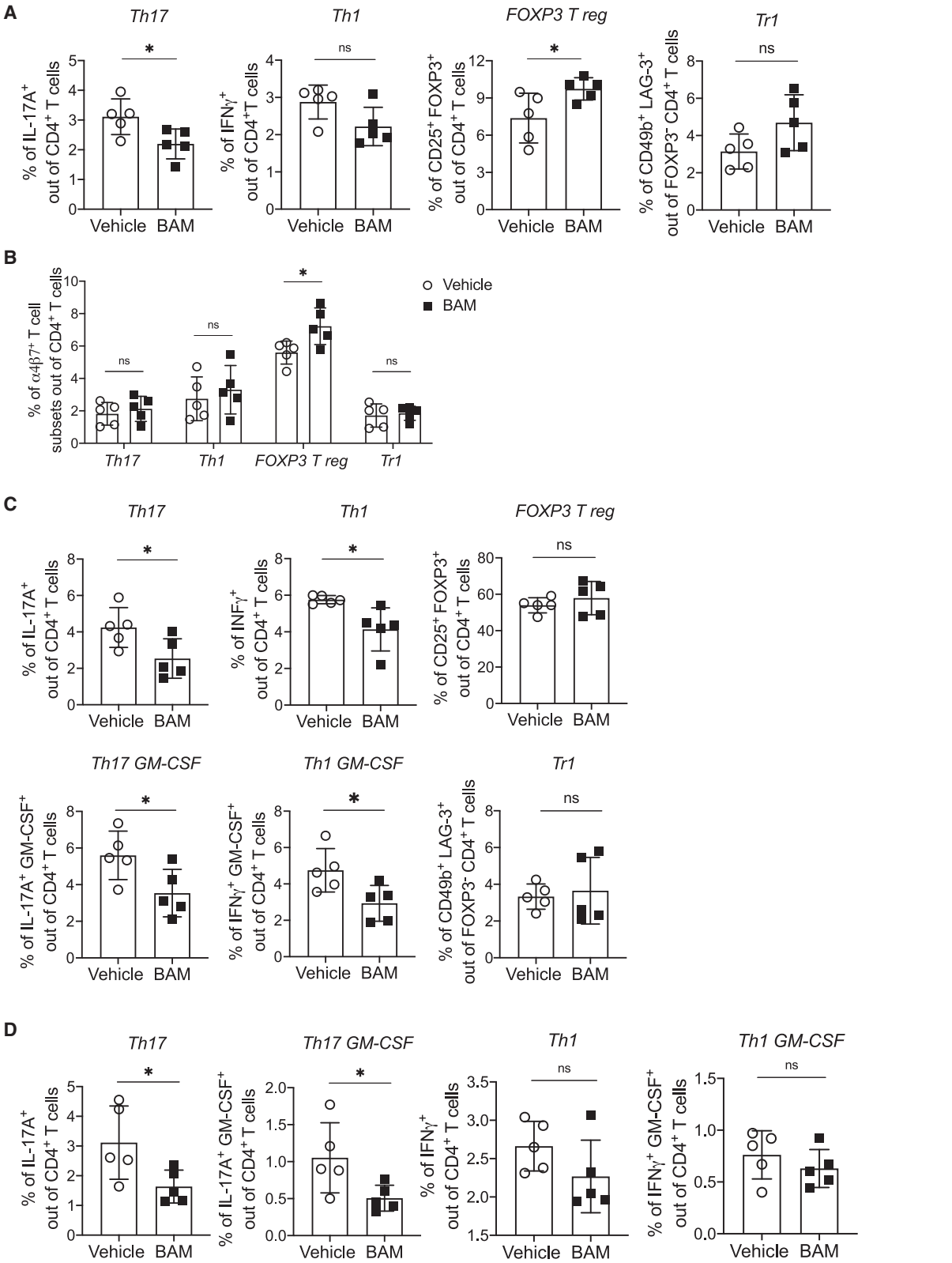

(legend on next page)

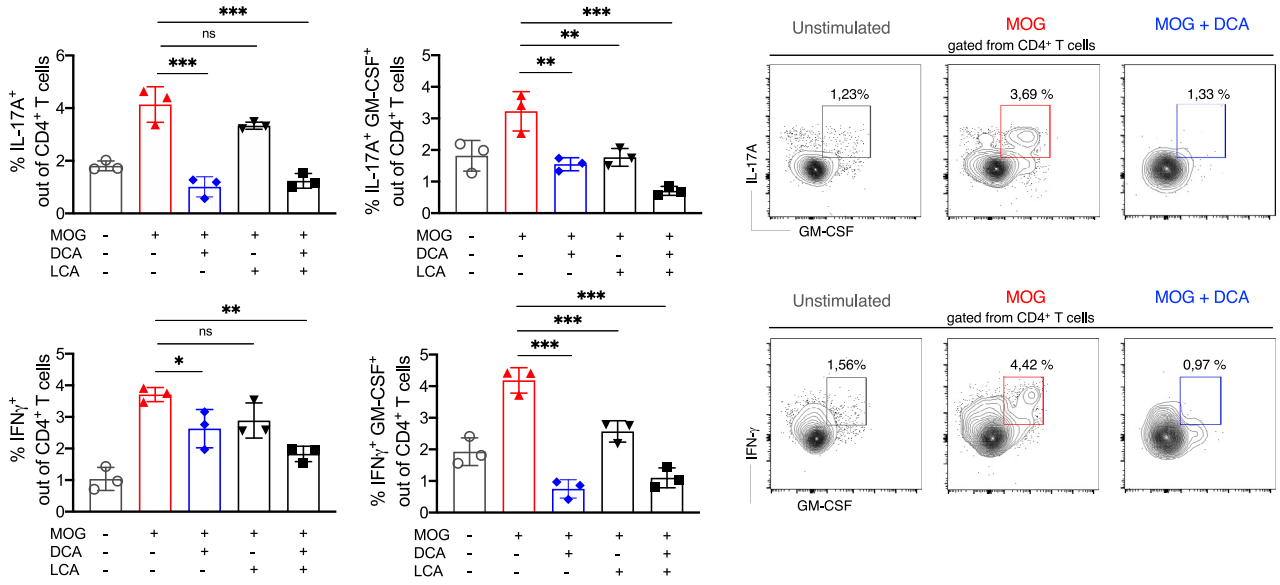

Figure 7. Immune regulatory DCA and LCA modulate the functional phenotype of myelin-specific T cells

Bone marrow-derived dendritic cells (DCs) were pulsed with the MOG35-55 peptide; stimulated with LPS (1 μg/mL) alone or in the presence of DCA, LCA, or DCA/LCA; and co-cultured for 72 h with naive CD4$^+$ T cells isolated from 2D2 TCR^{MOG} transgenic mice (DC:naive T cell ratio = 1:5, $n = 3$ per group). Representative flow cytometry plots (*right*) and bar graphs with individual values expressing the mean percentages ± SD (*left*) of Th17 (CD4$^+$ IL-17A$^+$), Th1 (CD4$^+$ IFN-γ$^+$), and GM-CSF$^+$ Th17 and Th1 cells out of total CD4$^+$ T cells from triplicate wells. One representative experiment out of two is shown. One-way ANOVA was used, followed by Dunnett's test for multiple comparisons. *$p < 0.05$; **$p < 0.01$; ***$p < 0.001$; ns, not significant.

A pioneer study showed that obeticholic acid, a synthetic BA agonist of the FXR, attenuates EAE by suppressing lymphocyte activation and release of inflammatory cytokines,[41] thus suggesting that the biliary network could have an immune regulatory function in CNS autoimmunity. Another study reported alteration of the BA metabolism in MS patients, particularly on those affected by the progressive form of the disease[42] and in RR models of EAE[43]; however, those studies focused their attention on BAMs such as tauroursodeoxycholic acid playing a direct neuroprotective effect on astrocytes and microglia rather than on immune regulatory secondary BAMs such as DCA and LCA. Here, in RRMS patients, we found a specific defect of secondary BAMs such as DCA that play fundamental immune regulatory function directly acting on immune cells and modulating the Teff/Treg cell ratio.

Importantly, our data demonstrated that the reduced intestinal concentration of immune regulatory BAMs is due to a highly significant reduction of the overall frequency of bacterial sequences that codify for enzymes crucial for secondary BAMs production. In line with this view, in RRMS patients, we found a reduction of bacteria that release key enzymes involved in 7-α-dehydroxylation, the enzymatic reaction that produces immune regulatory DCA, the secondary BAM that we found reduced in the intestine of RRMS patients.

The immune regulatory role of secondary BAMs in humans has been poorly investigated, and existing data mostly relate to the potential tolerogenic and anti-inflammatory effect of secondary BAMs in the intestine. In fact, secondary BAMs were found reduced in individuals with gut inflammation and exerted direct anti-inflammatory effect on human intestinal cells (Caco-2 cells) *in vitro*.[24] Here, we show a reduced concentration of DCA in individuals affected by CNS autoimmunity suggesting that, in humans, immune regulatory BAMs play their immune regulatory action also in peripheral tissues distal from the intestine. Accordingly, some of the BAM-producing bacterial strains that we found reduced in RRMS patients such as *Bifidobacterium longum*, *Bifidobacterium pseudocatenulatum*, and *Christenesella minuta* were previously demonstrated as capable of promoting immune

Figure 6. Immune regulatory secondary bile acid metabolites (BAM) modulate peripheral immunity in EAE mice

(A) Percentages of CD4$^+$ T cells expressing IL-17A (Th17), IFN-γ (Th1), FOXP3 and CD25 (FOXP3$^+$ Treg), or LAG3 and CD49b (FOXP3$^-$ Tr1) in the lymph nodes draining the immunization site (DLN) of EAE mice supplemented with BAM or vehicle.

(B) Percentages of CD4$^+$ α4β7$^+$ T cells among Th17, Th1, FOXP3$^+$ Treg, and FOXP3$^-$ Tr1 cells in the DLN of BAM-treated EAE mice.

(C) Percentages of Th17, GM-CSF$^+$Th17, Th1, GM-CSF$^+$ Th1, FOXP3$^+$ Treg, and FOXP3$^-$ Tr1 cells in the CNS of BAM-treated or vehicle-treated EAE-immunized mice.

(D) Percentages of Th17, GM-CSF$^+$Th17, Th1, and GM-CSF$^+$ Th1 cells in cell cultures enriched for MOG-specific T cells obtained from lymphocytes isolated from DLN of EAE mice supplemented or not with BAM.

Bars represent the mean ± SD. ($n = 5$ mice per group). Unpaired t test was performed. Data are from one representative experiment out of two. *$p < 0.05$, **$p < 0.01$; ns, not significant. See also Figure S9.

tolerance and reducing inflammation in the intestine[27,28] but also in extra-intestinal tissues such as the skin in atopic dermatitis[29] and the joints in rheumatoid arthritis (RA).[30]

The importance of the immune regulatory action of secondary BAMs in RRMS was further demonstrated by our observation that the reduction of BAM-producing bacterial species with consequent low DCA concentration in the intestine of our RRMS cohort was associated with immune dysregulation and, specifically, with increased relative percentage of circulating effector Th17 cells. Previous reports in murine models of uveitis demonstrated that DCA is particularly effective in dampening inflammation by reducing effector Th17 cell differentiation.[19] Hence, our finding of a significantly higher percentage of Th17 cells in the peripheral blood of RRMS patients with reduced intestinal concentrations of DCA suggests a similar regulatory effect of DCA on Th17 cell differentiation in humans. The causal link between the intestinal metabolic profile (with low DCA concentration) and increased Th17 cell percentage in PBMCs of our RRMS patients was further suggested by our *in vitro* findings showing that fecal filtrates from RRMS patients induced higher Th17 cell differentiation on naive human T cells in comparison with those of HCs, an effect that was inhibited by addition of DCA. Immune regulatory secondary BAMs (i.e., DCA, LCA, ω-muricholic acid (MCA), and isoDCA) also promote FOXP3$^+$Treg cell differentiation.[20,22] In our RRMS cohort, we did not detect alteration in the FOXP3$^+$Treg cell percentage in the peripheral blood, and the addition of RRMS fecal filtrates to PBMCs did not reduce FOXP3$^+$ Treg cell expansion, thus arguing that concentrations of DCA have minimal effect on human FOXP3$^+$ Treg cells. However, it is possible that DCA concentration affects FOXP3$^+$Treg cell differentiation mostly at the intestinal level where other concomitant modulatory factors and microbiota-produced molecules are present. For example, under steady-state conditions, intestinal DCs release tolerogenic cytokines that promote Treg cell differentiation,[44] which are absent in the PBMC-microbiota *in vitro* cultures. Also, molecules released by enteric cells such as immune modulatory mucins could modulate the Teff/Treg cell ratio in the gut mucosa.[45] Overall our human data suggest that decreased intestinal concentration of DCA and the reduced relative abundance of BAM-producing bacteria in RRMS patients induce the immune dysregulation (i.e., increased percentage of Th17 cells in peripheral blood) that we described here and, potentially, the breakage of gut barrier integrity and impairment of gut mucosal immunity previously reported.[6,46]

Our results in humans are suggestive of a correlation between the defective microbiota-regulated BA network and the pathogenesis of RRMS. Our work in preclinical models established a causal link between the intestinal concentration of immune regulatory BAMs such as DCA and LCA and control of CNS autoimmunity. Additionally, our data shed light on the underlying mechanism and the geography of BAM-mediated protection from CNS autoimmunity. In EAE, myelin-reactive T cells bearing an effector Th17 phenotype are licensed to cross the blood-brain barrier and enter the CNS to trigger autoimmunity and myelin damage.[47] In EAE-immunized mice, myelin-reactive T cells are activated and acquire the effector Th17 phenotype in the peripheral DLNs from where they migrate to the CNS. Our finding of a reduction of effector Th17 but also Th1 and highly encephalitogenic GM-CSF$^+$Th17 and GM-CSF$^+$Th1 cells in the CNS of BAM-protected EAE mice suggests that a lower number of myelin-reactive T cells with an effector phenotype are differentiated in the lymph nodes draining the site of EAE immunization. This modulatory effect can be mediated by two mechanisms. On one hand, Treg cells may differentiate in the gut mucosa upon BAMs administration and travel to the DLNs (where an inflammatory T cell response is ongoing) to suppress effector Th17/Th1 differentiation. In line with this view, we found increased percentages of FOXP3$^+$ Treg cells of intestinal origin ($\alpha4^+\beta7^+$) in the DLNs of BAM-treated EAE mice. Alternatively, DCA/LCA could modulate the functional phenotype of DCs in the DLN thus reducing their capacity to prime effector myelin-reactive T cells. This idea is supported by our finding that BAM-modulated DCs have a reduced capacity to trigger MOG_{35-55}-specific effector GM-CSF$^+$Th17/Th1 cells. Our finding that administration of DCA/LCA at the time of onset of clinical signs of EAE cannot counter-regulate and suppress the disease occurrence further supports the idea that the modulatory effect of secondary BAMs acts primarily on reducing priming of myelin-reactive effector Th17/Th1 cells. In fact, at the time of occurrence of clinical signs of EAE the myelin-reactive T cells already have a strongly biased effector Th17 phenotype that cannot be reverted and/or suppressed by the intestinal differentiation of regulatory FOXP3$^+$ Treg cells and Tr1 cells induced by BAMs administration.

The functional phenotype of T cells toward an effector or regulatory type is determined at the time of antigenic stimulation; hence, we believe that the inhibition of acquisition of an effector Th17/cell phenotype by myelin-reactive T cells in DCA/LCA-treated mice takes place in the DLNs where those autoreactive T cells are primed in EAE-immunized mice. However, in transgenic models of RRMS in which EAE occurs spontaneously and not through immunization, myelin-reactive T cells are activated and differentiated toward a Th17 cell phenotype in the gut mucosa.[47–49] Hence, we cannot exclude that in humans the intestinal mucosa and/or mesenteric LN are the primary site of differentiation of myelin-reactive Th17 cells and that lower intestinal concentration of DCA that we found in RRMS patients could favor this process. In line with this view, we previously found an increased percentage of effector Th17 cells in the intestine of RRMS patients with high disease activity.[6]

Our findings could have important therapeutic implications in RRMS. BA metabolism and commensal BAM-producing bacteria could represent new therapeutic targets to promote immune tolerance, reduce intestinal differentiation of myelin-reactive Th17 cells, and prevent disease relapses in RRMS. Future preclinical studies should be performed to assess the best therapeutic approach to restore normal intestinal levels of immune regulatory BAMs by enhancing the relative abundance of BAM-producing bacteria either through nutritional approaches or by administration of BAM-producing bacterial consortia. Importantly, the protective effect of immune regulatory BAMs could be extended to other extra-intestinal autoimmune diseases characterized by immune dysregulation at the intestinal level such as IBD but also extra-intestinal autoimmune diseases such as type 1 diabetes and RA. In support to this idea, a recent

study showed that oral administration of the single probiotic, *Bifidobacterium pseudocatenulatum*, a BAMs producer (that is under-represented in our RRMS cohort), was sufficient to increase intestinal concentration of DCA/LCA and prevent autoimmune RA in mice by suppressing peripheral Th17/Th1 cell expansion while promoting FOXP3$^+$ Treg cell differentiation.[30] Despite the availability of numerous disease-modifying therapies DMTs in RRMS, a significant percentage of patients are refractory or only partially respond to those treatments and develop new relapses and neurological deficits.[50] Recent evidence indicates that a beneficial gut microbiota could enhance therapeutic response to DMTs.[5] Similarly, restoring immune homeostasis and reducing effector Th17 cell differentiation by increasing intestinal concentration of immune regulatory BAMs could have a protective effect and enhance therapeutic responses to DMTs in RRMS patients.

Limitations of the study

The first limitation of our study is represented by the cohorts of MS patients and HCs that were limited in number and restricted to a single geographical area. Our observation of a reduction of BAM-producing bacteria and intestinal DCA concentration should be validated in larger cohorts of MS patients from different geographical regions. Second, we extrapolated the functional profiling of the human gut microbiota from the whole-genome sequencing data; however, our finding of a lower representation of BAM-producing bacteria that release enzymes involved in the multistep pathway of 7-α-dehydroxylation that is crucial to produce DCA should be confirmed by transcriptomic data. Third, we demonstrated that addition of secondary DCA or LCA to bone marrow-derived DCs *in vitro* reduced their capacity to trigger differentiation of autoimmune MOG-specific effector Th1 and Th17 cells; however, additional experiments are necessary to clarify the mechanisms responsible for BAM-mediated modulation of autoimmunity in the CNS.

RESOURCE AVAILABILITY

Lead contact

Further information and requests for resources and reagents should be directed to and will be fulfilled by the lead contact, Marika Falcone (falcone.marika@hsr.it).

Materials availability

This study did not generate new unique reagents.

Data and code availability

All data, code, and materials used in the analysis will be available in some form to any researcher for purposes of reproducing or extending the analysis. There is no restriction (MTA) on materials used in this study. Microbiota WGS sequencing data and UPLC/MS metabolomic data for all samples are deposited with the respective accession number in NCBI GEO repository: GEO: GSE233771 and Zenodo platform: https://doi.org/10.5281/zenodo.13318959, respectively, and are publicity available as of the date of publication. Accession numbers are also listed in the key resources table. Microscopy data reported in this paper will be shared by the lead contact upon request. This paper does not report original code. Any additional information required to reanalyze the data reported in this paper is available from the lead contact upon request.

ACKNOWLEDGMENTS

We thank all the participants (MS patients and healthy controls) who kindly agreed to participate in this study and donate blood and stool samples for research purposes. This research work was funded by the National Multiple Sclerosis Society (NMSS), USA, grant RG-1807-31885 (M.F.). The graphical abstract was created in BioRender.

AUTHOR CONTRIBUTIONS

Conceptualization: M.A.C., R.F., and M.F.
Methodology: M.A.C., V.P., M.L.C., L.M., and A.A.
Investigation: M.A.C., F.M., V.P., L.M., A.F., A.M., F.A., R.P., and D.D.
Visualization: M.A.C., L.M., and M.F.
Funding acquisition: M.F.
Project administration: M.F.
Supervision: F.U., A.A., N.S., V.M., R.F., and M.F.
Writing – original draft: M.A.C. and M.F.
Writing – review and editing: F.M., F.A., A.A., F.U., and V.M.

DECLARATION OF INTERESTS

The authors declare no competing interests.

STAR★METHODS

Detailed methods are provided in the online version of this paper and include the following:

- KEY RESOURCES TABLE
- EXPERIMENTAL MODEL AND STUDY PARTICIPANT DETAILS
  - Mice
  - Human subjects
- METHOD DETAILS
  - Shotgun metagenomic analysis
  - Metabolomic analysis
  - PBMC isolation and flow cytometry
  - Culture of PBMC with human fecal filtrates
  - Oral treatments and induction of EAE
  - Histopathological analysis
  - Real-time qPCR on intestinal tissue
  - Isolation of immune cells from murine tissues and flow cytometry
  - MOG-specific T cell recall assay
  - Dendritic cell generation and cell culture
- QUANTIFICATION AND STATISTICAL ANALYSIS

SUPPLEMENTAL INFORMATION

Supplemental information can be found online at https://doi.org/10.1016/j.xcrm.2025.102028.

Received: February 21, 2024
Revised: September 25, 2024
Accepted: February 21, 2025
Published: March 17, 2025

REFERENCES

1. Axisa, P.P., and Hafler, D.A. (2016). Multiple sclerosis: genetics, biomarkers, treatments. Curr. Opin. Neurol. *29*, 345–353.
2. Pröbstel, A.K., and Baranzini, S.E. (2018). The Role of the Gut Microbiome in Multiple Sclerosis Risk and Progression: Towards Characterization of the "MS Microbiome. Neurotherapeutics *15*, 126–134.
3. Kadowaki, A., and Quintana, F.J. (2020). The Gut-CNS Axis in Multiple Sclerosis. Trends Neurosci. *43*, 622–634.

4. Correale, J., Hohlfeld, R., and Baranzini, S.E. (2022). The role of the gut microbiota in multiple sclerosis. Nat. Rev. Neurol. *18*, 544–558.
5. iMSMS Consortium Electronic address sergiobaranzini@ucsfedu; iMSMS Consortium (2022). Gut microbiome of multiple sclerosis patients and paired household healthy controls reveal associations with disease risk and course. Cell *185*, 3467–3486.e16.
6. Cosorich, I., Dalla-Costa, G., Sorini, C., Ferrarese, R., Messina, M.J., Dolpady, J., Radice, E., Mariani, A., Testoni, P.A., Canducci, F., et al. (2017). High frequency of intestinal TH17 cells correlates with microbiota alterations and disease activity in multiple sclerosis. Sci. Adv. *3*, e1700492.
7. Wekerle, H. (2017). Nature, nurture, and microbes: The development of multiple sclerosis. Acta Neurol. Scand. *136*, 22–25.
8. Moles, L., Delgado, S., Gorostidi-Aicua, M., Sepúlveda, L., Alberro, A., Iparraguirre, L., Suárez, J.A., Romarate, L., Arruti, M., Muñoz-Culla, M., et al. (2022). Microbial dysbiosis and lack of SCFA production in a Spanish cohort of patients with multiple sclerosis. Front. Immunol. *13*, 960761.
9. Gaetani, L., Boscaro, F., Pieraccini, G., Calabresi, P., Romani, L., Di Filippo, M., and Zelante, T. (2020). Host and Microbial Tryptophan Metabolic Profiling in Multiple Sclerosis. Front. Immunol. *11*, 157.
10. Haghikia, A., Jörg, S., Duscha, A., Berg, J., Manzel, A., Waschbisch, A., Hammer, A., Lee, D.H., May, C., Wilck, N., et al. (2015). Dietary Fatty Acids Directly Impact Central Nervous System Autoimmunity via the Small Intestine. Immunity *43*, 817–829.
11. Rothhammer, V., Mascanfroni, I.D., Bunse, L., Takenaka, M.C., Kenison, J.E., Mayo, L., Chao, C.C., Patel, B., Yan, R., Blain, M., et al. (2016). Type I interferons and microbial metabolites of tryptophan modulate astrocyte activity and central nervous system inflammation via the aryl hydrocarbon receptor. Nat. Med. *22*, 586–597.
12. Su, X., Gao, Y., and Yang, R. (2023). Gut microbiota derived bile acid metabolites maintain the homeostasis of gut and systemic immunity. Front. Immunol. *14*, 1127743.
13. Wahlström, A., Sayin, S.I., Marschall, H.U., and Bäckhed, F. (2016). Intestinal Crosstalk between Bile Acids and Microbiota and Its Impact on Host Metabolism. Cell Metab. *24*, 41–50.
14. Cai, J., Sun, L., and Gonzalez, F.J. (2022). Gut microbiota-derived bile acids in intestinal immunity, inflammation, and tumorigenesis. Cell Host Microbe *30*, 289–300.
15. Ridlon, J.M., Kang, D.J., Hylemon, P.B., and Bajaj, J.S. (2014). Bile acids and the gut microbiome. Curr Opin Gastroen *30*, 332–338.
16. Gerard, P. (2013). Metabolism of cholesterol and bile acids by the gut microbiota. Pathogens *3*, 14–24.
17. Ridlon, J.M., Kang, D.J., and Hylemon, P.B. (2006). Bile salt biotransformations by human intestinal bacteria. J. Lipid Res. *47*, 241–259.
18. Hang, S., Paik, D., Yao, L., Kim, E., Trinath, J., Lu, J., Ha, S., Nelson, B.N., Kelly, S.P., Wu, L., et al. (2019). Bile acid metabolites control TH17 and Treg cell differentiation. Nature *576*, 143–148.
19. Hu, J., Wang, C., Huang, X., Yi, S., Pan, S., Zhang, Y., Yuan, G., Cao, Q., Ye, X., and Li, H. (2021). Gut microbiota-mediated secondary bile acids regulate dendritic cells to attenuate autoimmune uveitis through TGR5 signaling. Cell Rep. *36*, 109726.
20. Song, X., Sun, X., Oh, S.F., Wu, M., Zhang, Y., Zheng, W., Geva-Zatorsky, N., Jupp, R., Mathis, D., Benoist, C., and Kasper, D.L. (2020). Microbial bile acid metabolites modulate gut RORgamma(+) regulatory T cell homeostasis. Nature *577*, 410–415.
21. Pols, T.W.H., Puchner, T., Korkmaz, H.I., Vos, M., Soeters, M.R., and de Vries, C.J.M. (2017). Lithocholic acid controls adaptive immune responses by inhibition of Th1 activation through the Vitamin D receptor. PLoS One *12*, e0176715.
22. Campbell, C., McKenney, P.T., Konstantinovsky, D., Isaeva, O.I., Schizas, M., Verter, J., Mai, C., Jin, W.B., Guo, C.J., Violante, S., et al. (2020). Bacterial metabolism of bile acids promotes generation of peripheral regulatory T cells. Nature *581*, 475–479.
23. Biagioli, M., Carino, A., Cipriani, S., Francisci, D., Marchianò, S., Scarpelli, P., Sorcini, D., Zampella, A., and Fiorucci, S. (2017). The Bile Acid Receptor GPBAR1 Regulates the M1/M2 Phenotype of Intestinal Macrophages and Activation of GPBAR1 Rescues Mice from Murine Colitis. J. Immunol. *199*, 718–733.
24. Duboc, H., Rajca, S., Rainteau, D., Benarous, D., Maubert, M.A., Quervain, E., Thomas, G., Barbu, V., Humbert, L., Despras, G., et al. (2013). Connecting dysbiosis, bile-acid dysmetabolism and gut inflammation in inflammatory bowel diseases. Gut *62*, 531–539.
25. Sinha, S.R., Haileselassie, Y., Nguyen, L.P., Tropini, C., Wang, M., Becker, L.S., Sim, D., Jarr, K., Spear, E.T., Singh, G., et al. (2020). Dysbiosis-Induced Secondary Bile Acid Deficiency Promotes Intestinal Inflammation. Cell Host Microbe *27*, 659–670e5.
26. Sun, L., Zhang, Y., Cai, J., Rimal, B., Rocha, E.R., Coleman, J.P., Zhang, C., Nichols, R.G., Luo, Y., Kim, B., et al. (2023). Bile salt hydrolase in non-enterotoxigenic *Bacteroides* potentiates colorectal cancer. Nat. Commun. *14*, 755.
27. Kropp, C., Le Corf, K., Relizani, K., Tambosco, K., Martinez, C., Chain, F., Rawadi, G., Langella, P., Claus, S.P., and Martin, R. (2021). The keystone bacterium *Christensenella minuta* DSM 22607 displays anti-inflammatory properties both in vitro and in vivo. Sci. Rep. *11*, 11494.
28. Yao, S., Zhao, Z., Wang, W., and Liu, X. (2021). *Bifidobacterium Longum*: Protection against Inflammatory Bowel Disease. J. Immunol. Res. *2021*, 8030297.
29. Fang, Z., Pan, T., Li, L., Wang, H., Zhu, J., Zhang, H., Zhao, J., Chen, W., and Lu, W. (2022). *Bifidobacterium longum*-mediated tryptophan metabolism to improve atopic dermatitis via the gut-skin axis. Gut Microbes *14*, 2044723.
30. Zhao, Q., Ren, H., Yang, N., Xia, X., Chen, Q., Zhou, D., Liu, Z., Chen, X., Chen, Y., Huang, W., et al. (2023). *Bifidobacterium pseudocatenulatum*-mediated Bile Acid Metabolism to Prevent Rheumatoid Arthritis via the Gut-Joint Axis. Nutrients *15*, 255.
31. Ridlon, J.M., Kang, D.J., and Hylemon, P.B. (2010). Isolation and characterization of a bile acid inducible 7-alpha-dehydroxylating operon in *Clostridium hylemonae* TN271. Anaerobe *16*, 137–146.
32. Hirano, S., Nakama, R., Tamaki, M., Masuda, N., and Oda, H. (1981). Isolation and characterization of thirteen intestinal microorganisms capable of 7-alpha-dehydroxylating bile acids. Appl. Environ. Microbiol. *41*, 737–745.
33. Kitahara, M., Takamine, F., Imamura, T., and Benno, Y. (2001). *Clostridium hiranonis sp. nov.*, a human intestinal bacterium with bile acid 7alpha-dehydroxylating activity. Int. J. Syst. Evol. Microbiol. *51*, 39–44.
34. Mechelli, R., Romano, S., Romano, C., Morena, E., Buscarinu, M.C., Bigi, R., Bellucci, G., Reniè, R., Pellicciari, G., Salvetti, M., and Ristori, G. (2021). MAIT Cells and Microbiota in Multiple Sclerosis and Other Autoimmune Diseases. Microorganisms *9*, 1132.
35. Contentti, E.C., Farez, M.F., and Correale, J. (2019). Mucosal-Associated Invariant T Cell Features and TCR Repertoire Characteristics During the Course of Multiple Sclerosis. Frontiers Immunol *10*, 2690.
36. Gibbons, J., Yoo, J.Y., Mutka, T., Groer, M., and Ho, T.T.B. (2021). A Pilot Study To Establish an In Vitro Model To Study Premature Intestinal Epithelium and Gut Microbiota Interactions. mSphere *6*, e0080621.
37. Lee, Y.K., Menezes, J.S., Umesaki, Y., and Mazmanian, S.K. (2011). Proinflammatory T-cell responses to gut microbiota promote experimental autoimmune encephalomyelitis. Proc. Natl. Acad. Sci. USA *108*, 4615–4622.
38. Nouri, M., Bredberg, A., Weström, B., and Lavasani, S. (2014). Intestinal barrier dysfunction develops at the onset of experimental autoimmune encephalomyelitis, and can be induced by adoptive transfer of auto-reactive T cells. PLoS One *9*, e106335.
39. Ponomarev, E.D., Shriver, L.P., Maresz, K., Pedras-Vasconcelos, J., Verthelyi, D., and Dittel, B.N. (2007). GM-CSF production by autoreactive

T cells is required for the activation of microglial cells and the onset of experimental autoimmune encephalomyelitis. J. Immunol. *178*, 39–48.

40. Fettig, N.M., and Osborne, L.C. (2021). Direct and indirect effects of microbiota-derived metabolites on neuroinflammation in multiple sclerosis. Microbes Infect. *23*, 104814.
41. Ho, P.P., and Steinman, L. (2016). Obeticholic acid, a synthetic bile acid agonist of the farnesoid X receptor, attenuates experimental autoimmune encephalomyelitis. Proc. Natl. Acad. Sci. USA *113*, 1600–1605.
42. Bhargava, P., Smith, M.D., Mische, L., Harrington, E., Fitzgerald, K.C., Martin, K., Kim, S., Reyes, A.A., Gonzalez-Cardona, J., Volsko, C., et al. (2020). Bile acid metabolism is altered in multiple sclerosis and supplementation ameliorates neuroinflammation. J. Clin. Investig. *130*, 3467–3482.
43. Mangalam, A., Poisson, L., Nemutlu, E., Datta, I., Denic, A., Dzeja, P., Rodriguez, M., Rattan, R., and Giri S. (2013). Profile of Circulatory Metabolites in a Relapsing-remitting Animal Model of Multiple Sclerosis using Global Metabolomics. J. Clin. Cell. Immunol. *4*, 3.
44. Coombes, J.L., and Powrie, F. (2008). Dendritic cells in intestinal immune regulation. Nat. Rev. Immunol. *8*, 435–446.
45. Shan, M., Gentile, M., Yeiser, J.R., Walland, A.C., Bornstein, V.U., Chen, K., He, B., Cassis, L., Bigas, A., Cols, M., et al. (2013). Mucus enhances gut homeostasis and oral tolerance by delivering immunoregulatory signals. Science *342*, 447–453.
46. Buscarinu, M.C., Cerasoli, B., Annibali, V., Policano, C., Lionetto, L., Capi, M., Mechelli, R., Romano, S., Fornasiero, A., Mattei, G., et al. (2017). Altered intestinal permeability in patients with relapsing-remitting multiple sclerosis: A pilot study. Mult. Scler. *23*, 442–446.
47. Kebir, H., Kreymborg, K., Ifergan, I., Dodelet-Devillers, A., Cayrol, R., Bernard, M., Giuliani, F., Arbour, N., Becher, B., and Prat, A. (2007). Human TH17 lymphocytes promote blood-brain barrier disruption and central nervous system inflammation. Nat. Med. *13*, 1173–1175.
48. Berer, K., Mues, M., Koutrolos, M., Rasbi, Z.A., Boziki, M., Johner, C., Wekerle, H., and Krishnamoorthy, G. (2011). Commensal microbiota and myelin autoantigen cooperate to trigger autoimmune demyelination. Nature *479*, 538–541.
49. Duc, D., Vigne, S., Bernier-Latmani, J., Yersin, Y., Ruiz, F., Gaïa, N., Leo, S., Lazarevic, V., Schrenzel, J., Petrova, T.V., and Pot, C. (2019). Disrupting myelin-specific Th17 cell gut homing confers protection in an adoptive transfer experimental autoimmune encephalomyelitis. Cell Rep. *29*, 378–390.e4.
50. Callegari, I., Derfuss, T., and Galli, E. (2021). Update on treatment in multiple sclerosis. Presse Med. *50*, 104068.
51. Wood, D.E., and Salzberg, S.L. (2014). Kraken: ultrafast metagenomic sequence classification using exact alignments. Genome Biol. *15*, R46.
52. Patil, I. (2021). Visualizations with statistical details: The 'ggstatsplot' approach. J. Open Source Softw. *6*, 3167.
53. Johnson, M., Zaretskaya, I., Raytselis, Y., Merezhuk, Y., McGinnis, S., and Madden, T.L. (2008). NCBI BLAST: a better web interface. Nucleic Acids Res. *36*, W5–W9.
54. Langmead, B., and Salzberg, S.L. (2012). Fast gapped-read alignment with Bowtie 2. Nat. Methods *9*, 357–359.
55. Thorvaldsdottir, H., Robinson, J.T., and Mesirov, J.P. (2013). Integrative Genomics Viewer (IGV): high-performance genomics data visualization and exploration. Brief Bioinform *14*, 178–192.
56. Tsugawa, H., Cajka, T., Kind, T., Ma, Y., Higgins, B., Ikeda, K., Kanazawa, M., VanderGheynst, J., Fiehn, O., and Arita, M. (2015). MS-DIAL: data-independent MS/MS deconvolution for comprehensive metabolome analysis. Nat. Methods *12*, 523–526.
57. Love, M.I., Huber, W., and Anders, S. (2014). Moderated estimation of fold change and dispersion for RNA-seq data with DESeq2. Genome Biol. *15*, 550.
58. Lutz, M.B., Kukutsch, N., Ogilvie, A.L., Rössner, S., Koch, F., Romani, N., and Schuler, G. (1999). An advanced culture method for generating large quantities of highly pure dendritic cells from mouse bone marrow. J. Immunol. Methods *223*, 77–92.

STAR★METHODS

KEY RESOURCES TABLE

REAGENT or RESOURCE	SOURCE	IDENTIFIER
Antibodies		
Anti-human CD127 Alexa Fluor 488	Invitrogen	Cat# 53-1278-42; RRID:AB_2744750
Anti-human Tbet PE-Cy5	Invitrogen	Cat# 15-5825-42; RRID:AB_2815071
Anti-human FOXP3 APC	Invitrogen	Cat# 17-4776-42; RRID:AB_1603280
Anti-human RORγt PE	Thermofisher	Cat# 12-6988-82; RRID:AB_1834470
Anti-human CD25 PE-Cy7	BD Pharmingen	Cat# 557741; RRID:AB_396847
Anti-human CD3 APC-Cy7	BD Pharmingen	Cat# 557757; RRID:AB_396863
Anti-human TCR Vα7.2 BV570	BD Horizon	Cat# 749487; RRID:AB_2873855
Anti-human CD161 BV711	BD Horizon	Cat# 563865; RRID:AB_2738457
Anti-human CD45 BUV395	BD Horizon	Cat# 563791; RRID:AB_2744400
Anti-human CD8 BUV805	BD Horizon	Cat# 612889; RRID:AB_2833078
Anti-human CRTH2 BV786	BD OptiBuild	Cat# 741016; RRID:AB_2740637
Anti-human CD4 BUV496	BD OptiBuild	Cat# 750591; RRID:AB_2874725
Anti-human TCRγδ BUV563	BD OptiBuild	Cat# 748534; RRID:AB_2872945
Anti-mouse CD45 BV510	BioLegend	Cat# 103137; RRID:AB_2561392
Anti-mouse CD4 Alexa Fluor 700	BioLegend	Cat# 116022; RRID:AB_2715957
Anti-mouse CD25 Alexa Fluor 488	BioLegend	Cat# 102017; RRID:AB_493334
Anti-mouse LAG3 PE-Cy7	BioLegend	Cat# 125226; RRID:AB_2715763
Anti-mouse CD49b APC-Cy7	BioLegend	Cat# 108920; RRID:AB_2561458
Anti-mouse FOXP3 eFluor450	Invitrogen	Cat# 48-5773-82; RRID:AB_1518812
Anti-mouse CD45 APC-eFluo780	Invitrogen	Cat# 47-0451-82; RRID:AB_1548781
Anti-mouse IL-17A Alexa Fluor 647	BD Pharmingen	Cat# 560184; RRID:AB_1645204
Anti-mouse IFN-γ PerCP-Cy5	BD Pharmingen	Cat# 560660; RRID:AB_1727533
Anti-mouse GM-CSF PE	BD Pharmingen	Cat# 554406; RRID:AB_395371
Anti-mouse LPAM-1 BV650	BD Pharmingen	Cat# 740493; RRID:AB_2740216
Anti-mouse CD3 FITC	BD Bioscience	Cat# 555274; RRID:AB_395698
Anti-mouse CD4 PerCP-Cy5.5	BD Bioscience	Cat# 550954; RRID:AB_393977
Anti-mouse IFN-γ V450	BD Bioscience	Cat# 560661; RRID:AB_1727534
Biological samples		
Human peripheral blood	This study	N/A
Human fecal samples	This study	N/A
Chemicals, peptides, and recombinant proteins		
Fixable Viability Dye eFluor506	Thermofisher	Cat# 65-0866-14;
Fixable Viability Dye Viakrome808	Beckman coulter	Cat# C36628;
Lympholyte®-H Cell Separation Media	Cederlane Laboratories	Cat# DVCL5020;
LCA	Sigma	Cat# L6250;
DCA	Sigma	Cat# D2510;
Corn oil	Sigma	Cat# C8267;
Incomplete Freund's adjuvant	Sigma-Aldrich	Cat# F5506;
Mycobacterium tuberculosis strain H37Ra	BD Difco	Cat# 231141;
Pertussis toxin	Q-TOX	Cat# QTXAG-108-500;
TRIzol	Life Technologies	Cat# 10296010;
Critical commercial assays		
DNA/RNA Shield Fecal Collection Tubes	ZYMO RESEARCH	Cat#R1101-E;

(*Continued on next page*)

Continued

REAGENT or RESOURCE	SOURCE	IDENTIFIER
QIAamp PowerFecal Pro DNA Kit	QIAGEN	Cat# 51804;
Nextera DNA Flex Library Preparation Kit	Illumina	Cat# 20018705;
FOXP3/Transcription Factor Staining Buffer Set	ThermoFisher	Cat# 00-5523-00;
Cytofix/Cytoperm kit	BD	Cat# 555280;
RNeasy Mini Kit	QIAGEN	Cat#74104;
SuperScript III First-Strand Synthesis System	Life Technologies	Cat#18080051;
SYBR Select Master Mix	Life Technologies	Cat# 4472908;
Lamina Propria Dissociation Kit, mouse	Miltenyi Biotec	Cat# 130-097-410;
Leukocytes Activation Cocktail with BD GolgiPlug™	BD Bioscience	Cat# 550583;
Mouse GM-CSF	Miltenyi Biotec	Cat# 130-095-746;
Mouse IL-4	Miltenyi Biotec	Cat# 130-097-757;
Lipopolysaccharide	Sigma-Aldrich	Cat# L2880;
Naive $CD4^+$ T cell isolation kit, mouse	Miltenyi Biotec	Cat# 130-104-453;
Deposited data		
Shotgun metagenomics, NCBI GEO repository	This paper	Accession ID GEO: GSE233771
UPLC/MS metabolomic data, Zenodo platform	This paper	https://doi.org/10.5281/zenodo.13318959.
Experimental models: Organisms/strains		
C57BL/6 mice	Charles River Laboratories	N/A
2D2 TCR^{MOG} tg mice	The Jackson Laboratory	N/A
Oligonucleotides		
Mouse Nr1h4 F: 5′- TCACCTGTGAGGGCTGCAAA - 3′	Invitrogen	N/A
Mouse Nr1h4 R: 3′- ACACTGGATTTCAGTTAACAAACCT - 5′	Invitrogen	N/A
Mouse Gpbar1 F: 5′- ATGGAGCCGGAACCATCAGG - 3′	Invitrogen	N/A
Mouse Gpbar1 R: 3′- CAGCAGATTGGCAAGCAGGG - 5′	Invitrogen	N/A
Mouse Nr1l1 F: 5′- GCCTCCAATTCGTGCAGACG - 3′	Invitrogen	N/A
Mouse Nr1l1 R: 3′- GGTCACAGAGGGGTCATCGG - 5′	Invitrogen	N/A
Mouse IL-6 F: 5′- ACAAAGCCAGAGTCCTTCAGAGA - 3′	Invitrogen	N/A
Mouse IL-6 R: 3′- AGGAGAGCATTGGAAATTGGGGT - 5′	Invitrogen	N/A
Mouse IL-18 F: 5′- CTTGGCCCAGGAACAATGGC - 3′	Invitrogen	N/A
Mouse IL-18R: 3′- CGGTTGTACAGTGAAGTCGGC - 5′	Invitrogen	N/A
Mouse IL-1b F: 5′- TGCCACCTTTTGACAGTGATGA - 3′	Invitrogen	N/A
Mouse IL-1b R: 3′- TGCCTGCCTGAAGCTCTTGT - 5′	Invitrogen	N/A
Mouse Tnfa F: 5′- CTGTAGCCCACGTCGTAGCA - 3′	Invitrogen	N/A
Mouse Tnfa R: 3′- GTGTGGGTGAGGAGCACGTA - 5′	Invitrogen	N/A
Mouse IL-10 F: 5′- TGGGTTGCCAAGCCTTATCG - 3′	Invitrogen	N/A
Mouse IL-10 R: 3′- CTCTTCACCTGCTCCACTGC - 5′	Invitrogen	N/A
Mouse Rpl32 F: 5′- AAGCGAAACTGGCGGAAAC - 3′	Eurofins	N/A
Mouse Rpl32 R: 3′- TAACCGATGTTGGGCATCAG - 5	Eurofins	N/A
Software and algorithms		
BMTagger		https://ftp.ncbi.nlm.nih.gov/pub/agarwala/bmtagger/
Kraken2	Wood, D.E. & Salzberg, S.L.[51]	https://www.ncbi.nlm.nih.gov/genome/
Vegan R package		https://cran.r-project.org/web/packages/vegan
ggstatsplot R package	Patil, I.[52]	
ggplot2 R package		https://ggplot2.tidyverse.org
NCBI BLAST	Johnson, M. et al.[53]	https://www.bioinformatics.babraham.ac.uk/projects/fastqc/

(*Continued on next page*)

Continued

REAGENT or RESOURCE	SOURCE	IDENTIFIER
Bowtie2	Langmead B. and Salzberg S.L.[54]	http://bowtie-bio.sourceforge.net/bowtie2/index.shtml
Integrative Genomics Viewer	Thorvaldsdottir, H., Robinson, J. T. & Mesirov, J. P[55]	https://www.igv.org
MS-DIAL	Tsugawa, H. et al.[56]	http://prime.psc.riken.jp/compms/msdial/main.html
FlowJo version 10.8.1	FlowJo	https://www.flowjo.com/
Graphpad Prism version 8.0	GraphPad Software	https://www.graphpad.com
DESeq2 R package	Love, M. I., Huer, W. & Anders, S.[57]	https://bioconductor.org/packages/release/bioc/html/DESeq2.html

EXPERIMENTAL MODEL AND STUDY PARTICIPANT DETAILS

Mice

6-8 week-old female C57BL/6 mice were purchased from Charles River Laboratories and used for *in vivo* experiments. 10-12 week-old female 2D2 TCR^{MOG} transgenic mice (C57BL/6 background) were used for *ex vivo* experiments. All mice were maintained in specific-pathogen free conditions in the animal facility at the San Raffaele Scientific Institute (Milan, Italy). All experiments were conducted in accordance with the rules of the Italian Ministry of Health and approved by the Institutional Animal Care and Use Committee of the San Raffaele Scientific Institute.

Human subjects

The study cohort included 20 RRMS patients and 20 healthy controls (HC). In the RRMS group we allocated patients with a diagnosis of relapsing-remitting MS as defined according to the 2017 McDonald criteria. In the healthy control (HC) group we allocated individuals with no MS and no other pathology including autoimmune diseases. The RRMS group includes individuals with age between 24 and 70 years with 17 females and 3 males while the HC group includes subject with age between 22 and 55 years with 8 females and 12 males. Information regarding mean age and sex of the two group is shown in Table S2. Our multivariate analysis (Figure 2B) demonstrated that sex had no influence on the results of our study (DCA concentration in human stool samples). All individuals signed a written informed consent and were aware that they donated biological samples for research purposes. Protocols for collection and analysis of the human samples (blood and fecal material) were approved by the institutional Ethical Committee of the IRCCS Ospedale San Raffaele (Protocol: MS-GUT2019), Milan, Italy. Exclusion criteria for both HC and RRMS patients were the following: treatment with antibiotics or corticosteroids in the 3 months before the date of stool sample collection, clinical history of gastroenteritis, gastric ulcer, irritable bowel syndrome, celiac disease, inflammatory bowel disease, gastric and colorectal cancer.

METHOD DETAILS

Shotgun metagenomic analysis

For metagenomic analysis, each subject enrolled in this study provided fecal samples that were collected in DNA/RNA Shield Fecal collection Tubes (Zymo research). DNA was extracted from fecal samples using the QIAamp powerFecal Pro DNA Kit (Qiagen) following the manufacturer's instructions. Sequencing libraries were prepared using the Nextera DNA Flex Library Preparation Kit (Illumina), following the manufacturer's instructions. Sequencing was performed on the Illumina NovaSeq 6000 platform following the manufacturer's protocol on an S4 flow cell for 150bp paired-end. For human gut microbiota analysis, microbial reads (55.1 ± 16.8 $X10^6$ reads/sample) were discriminated against human reads with BMTagger (ftp.ncbi.nlm.nih.gov/pub/agarwala/bmtagger/). To perform the analysis at order/family/species levels, reads were mapped to the collection of all available genomes (https://www.ncbi.nlm.nih.gov/genome/) with Kraken2 for exact alignment of k-mers and accurate read classification.[43] Before statistical analysis, classified reads were double-checked with FastQC (https://www.bioinformatics.babraham.ac.uk/projects/fastqc/) to confirm quality filtering and adaptor trimming, and then submitted to BLAST[44] to exclude possible artifacts resulting from the *in-silico* analysis. Read calls were confirmed by manually aligning Kraken2 classified reads to the respective genomes with Bowtie2[45] and visualizing the resulting BAM alignments with the Integrative Genomics Viewer (IGV).[46] 7376 bacterial species were identified. Data were deposited in the NCBI GEO repository with Accession ID GSE233771 (https://www.ncbi.nlm.nih.gov/geo/query/acc.cgi?acc=GSE233771).

Metabolomic analysis

Snap-frozen stool samples were used for metabolomic analysis. 300 μL of isopropanol were added to 100 mg of fecal samples along with Internal Standards (IS). 1 μg of each IS (Tryptophan(indole)-d5; Phenylalanine-15N; Stearic Acid-d3; Sphingosine(*d*18-1)d7;

Glucosyl(β)sphingosine-d5; C16-Glucosylcarbamide-d3; Phosphoetanolamine-d4) were added to each sample. Samples were vortexed for 2 min to obtain a homogeneous mixture, sonicated on ice for 5 min, then centrifuged at 14000g for 15 min at 4°C. The supernatants were filtered with 0.45 μm filter. After filtration the samples were diluted 1:1 with isopropanol. The metabolomic profile of human feces was analyzed by UPLC (UPLC 1290 system, Agilent Technologies) directly connected to mass spectrometry (TripleTOF 5600+ mass spectrometer, SCIEX equipped with an electrospray ionization source (ESI). Quality control (QC) samples were prepared as pool of all the samples, by mixing equal volume of each extracted sample and analyzed within the queue. Chromatographic separations occurred on an Acquity BEH AMIDE (100 × 2.1 mm, 1.7 μm, Waters) capillary column. A gradient of solvent A (acetonitrile containing 0.1% formic acid) and B (water containing 0.1% formic acid) was used to achieve separation (600 μL/min as flow rate): 1 min at 2% B, from 2% B to 60% B in 10 min, 2 min hold at 60% B, in 0.50 min–2% B, 3 min hold at 2% B. The column temperature was set at 40°C, while the autosampler was set at 4°C. 8 μL of samples were injected. Full scan spectra were acquired in the mass range from m/z 50 to 500 with an SWATH modality acquisition of 10 windows. The source parameters were: Gas 1: 33 psi, Gas 2: 58 psi, Curtain gas: 35 psi, Temperature: 500°C and ISVF (IonSpray Voltage Floating): 5500 V (−4500 V for negative polarity), DP: 80 V, CE: 35 V with a spread of 15V. The same samples were also analyzed by using reverse phase (RP) Acquity HSS T3 C18 column (100 × 2.1 mm, 1.8 μm, Waters). A gradient of solvent A (water containing 0.1% formic acid) and B (acetonitrile containing 0.1% formic acid) was used to achieve separation (600 μL/min as flow rate): 1 min at 2% B, from 2% B to 95% B in 14 min, 5 min hold at 95% B, in 0.50 min–2% B, 5 min hold at 2% B. 10 μL of samples were injected. Full scan spectra were acquired in the mass range from m/z 50 to 850 with an SWATH modality acquisition of 16 windows. The source parameters were: Gas 1: 33 psi, Gas 2: 58 psi, Curtain gas: 35 psi, Temperature: 500°C and ISVF (IonSpray Voltage Floating): 5500 V (−4500 V for negative polarity), DP: 80 V, CE: 35 V with a spread of 15V. The.wiff files acquired on the mass spectrometer were converted to.abf files using Reifycs Analysis Base File Converter and analyzed with MS-DIAL v. 4.7[47] for peak picking, gap filling, alignment. The identification was performed using MS/MS Positive Public library v. 14.0, MS/MS Negative Public library v. 14.0. The MS-DIAL output was manually inspected to verify the annotation of the metabolites. A total of 379 compounds were identified. Data normalization, based on 23 quality control (QC) samples, was carried out using the LOWESS methods, which is an integral part of MS-DIAL software. Data were deposited at the Zenodo platform with https://doi.org/10.5281/zenodo.13318959. (https://zenodo.org/badge/DOI/10.5281/zenodo.13318959.svg).

PBMC isolation and flow cytometry

Paired blood samples from all the individuals (RRMS and HC) enrolled in the study were collected in EDTA-vacutainers and immediately processed for peripheral blood mononuclear cells (PBMC) isolation. PBMC were isolated from whole blood by density gradient centrifugation using the Lympholyte-H Cell Separation Media (Cederlane Laboratories) according to the manufacturer's instructions. Following isolation, cell pellet was suspended in FBS supplemented with 10% Dimethyl Sulfoxide (DMSO), aliquoted and cryopreserved in liquid nitrogen for long-term storage. On the day of analysis, cryopreserved PBMC were thawed, washed with RPMI-1640 containing 10% FBS and counted. Approximately 1 × 10^6 cells were transferred into a 96-well U-bottom plate and incubated for 20 min at RT with 10% heat-inactivated human serum (Human Serum Type AB male, Euroclone) as Fc receptor blocking agent. Subsequently, cells were washed once in PBS by centrifugation (400 × g, 5 min, RT) and subjected to the following staining procedure. Cells were first stained with Fixable Viability dye eFluor506 (ThermoFisher) diluted in PBS (1:500) for live/dead cell discrimination, and then incubated 20 min at 4°C in the dark with a combination of fluorochrome-conjugated surface antibodies in staining buffer. The staining of nuclear transcription factors was performed using the FOXP3/Transcription Factor Staining Buffer Set (ThermoFisher). In brief, after surface staining, cells were incubated with freshly prepared fixation/permeabilization solution for 45 min at 4°C, washed with Perm/Wash buffer, and then stained for 30 min at RT with a mixture of fluorochrome-conjugated anti-human antibodies against FOXP3, Tbet and RORγt diluted in a 1:1 mix of 1X Perm/Wash buffer and Brilliant Stain Buffer. After intracellular staining, cells were suspended in 200 μL of FACS buffer for subsequent analysis. All the antibodies used are listed in the key resources table: Alexa Fluor 488 anti-human CD127 (Invitrogen), PE-Cy5 anti-human Tbet (Invitrogen), APC anti-human FOXP3 (Invitrogen), PE anti-human RORγt (ThermoFisher), PE-Cy7 anti-human CD25 (BD Pharmingen), APC-Cy7 anti-human CD3 (BD Pharmingen), TCRVα7.2 BV570 anti-human (BD Horizon), BV711 anti-human CD161 (BD Horizon), BUV395 anti-human CD45 (BD Horizon), BUV805 anti-human CD8 (BD Horizon), BV786 anti-human CRTH2 (BD OptiBuild), BUV496 anti-human CD4 (BD OptiBuild), BUV563 anti-human TCRγδ (BD OptiBuild). All samples were acquired on BD FACSymphony A5 flow cytometer (BD Biosciences) and analyzed with FlowJo software (v.10.8.1) using unstained and single-stained compensation beads as compensation controls. Fluorescence minus one (FMO) as well as non-stimulated cells were used as negative controls. See Figure S8 for gating strategy of human PBMCs.

Culture of PBMC with human fecal filtrates

Fecal filtrates were prepared from stool samples of RRMS patients and HC, as previously described with minor modifications.[28] Briefly, thawed stools were diluted in sterile PBS to a final concentration of 100 mg/mL and vigorously vortexed until homogenized. The stool mixture was smashed on 40mm filters and the flow-through spun at 4.000g and 4°C for 10 min. Supernatant was collected and filtered using a 0.2 mm sterile filter. Total PBMCs isolated from one healthy donor were cultured (2X10^5/well) in the presence or absence of sterile fecal filtrates in complete RPMI-1640. After 72h, cells were recovered and FACS analyzed. In separate experiments, human healthy PBMCs were cultured in the presence of sterile fecal filtrates isolated from RRMS patients with or without the presence of 10 μM DCA.

Oral treatments and induction of EAE

After one week of acclimatization 7-week-old female C57BL/6 mice were orally administered daily with an emulsion of lithocholic acid (Sigma-Aldrich) and/or deoxycholic acid (Sigma-Aldrich) (10 mg/kg) or the vehicle corn oil seven days before EAE immunization (prophylaxis regimen). For therapeutic regimen experiments, mice were orally supplemented with DCA/LCA or corn oil at onset of the first clinical signs of disease (day 10 after immunization). EAE was induced by subcutaneous injection of an emulsion containing 200 μg of MOG_{35-55} peptide (Espikem) in incomplete Freund's adjuvant (Sigma-Aldrich) supplemented with 4 mg/mL Mycobacterium tuberculosis (strain H37Ra; BD Difco), herein referred as CFA. Pertussis toxin (500 ng, Q-TOX) was injected intravenously on the day of EAE immunization and 2 days later. Mice were daily weighed and scored for clinical signs of EAE up to the day of sacrifice. Clinical assessment of EAE was performed according to the following scoring criteria: 0, healthy; 1, limb tail; 2, ataxia and/or paresis of hindlimbs; 3, paralysis of hindlimbs and/or paresis of forelimbs; 4, tetraparalysis; and 5, moribund or death. EAE mice treated in prophylaxis were sacrificed for MOG-antigen recall assay at day 18 post-immunization (p.i.) and for the analysis of tissue-infiltrating lymphocytes at day 20–24 p.i. For those supplemented with BAM in therapeutic regimen, EAE mice were sacrificed at day 16 p.i.

Histopathological analysis

For neuropathological analysis, mice were transcardially perfused with 4% paraformaldehyde. Spinal cord tissues were isolated and post-fixed in the same fixative overnight, washed in PBS and then embedded in paraffin. Sections were stained with haematoxylin and eosin (H&E), Luxol fast blue (Kluver Barrera) and Bielschowsky staining methods to reveal the perivascular inflammatory infiltrates, demyelinated areas, and axonal loss, respectively. Neuropathological findings were quantified on an average of 10 complete cross-sections of spinal cord per mouse collected at 9 different levels of the spinal cord. The number of inflammatory infiltrates were calculated and expressed as the number of inflammatory infiltrates per mm^2; demyelinated areas and axonal loss were expressed as percentage of damaged area per mm^2.

Real-time qPCR on intestinal tissue

Upon sacrifice, colonic tissues were flushed with PBS, opened longitudinally, and one tissue fragment was placed in 500 μL of TRIzol reagent (Life Technologies). Tissues were homogenized by using TissueRuptor (QIAGEN) and RNA was extracted by adding 10 μL of chloroform, precipitating the aqueous phase with 300 μL of 70% ethanol, and purifying RNA with RNeasy Mini Ki (QIAGEN). RNA was retrotranscribed with SuperScript III First-Strand Synthesis System following manufacturer's instructions (life Technologies). Real-time qPCR was performed on a Viia 7 real-time PCR System (Life Technologies) with SYBR Select Master Mix (Life Technologies) using specific primers listed in the key resource table. Transcript levels of individual genes were normalized to the expression of the housekeeping gene ribosomal protein L32 (RPL32).

Isolation of immune cells from murine tissues and flow cytometry

At the indicated time of sacrifice, mice were anesthetized and transcardially perfused with PBS and the intestine, DLN (inguinal and axillary) and CNS (brain and spinal cord tissues) were collected. Lymphocytes were isolated from the intestinal lamina propria using the Lamina Propria Dissociation Kit following manufacturer's instructions (Miltenyi Biotec). For CNS cell isolation, both brain and spinal cord tissues were cut into small pieces, homogenized and incubated in HBSS (w Calcium and Magnesium) containing 0.4 mg/mL Collagenase Type IV (Sigma) and 10% FBS at 37°C for 30 min. The digested tissues were washed and resuspended in 9 mL PBS 1X in a 15 mL-Falcon tubes. A 90% Percoll (GE Healthcare) solution was prepared, and 4.5 mL of such solution were overlaid on 9 mL of PBS 1X containing the digested tissues. Percoll gradient separation was performed by centrifugation at 10800 rpm for 30 min at 4°C. After the centrifuge, the layer of myelin debris was aspirated and eliminated while the rest of the sample containing CNS immune cells was resuspended in PBS. Immune cells from DLN were isolated by mechanical disruption of the tissue. Immune cells isolated from the different organs were stimulated for 4h with Leukocytes Activation Cocktail with BD GolgiPlug following manufacturer's instruction (BD Biosciences) and stained for flow cytometry analysis. Briefly, cells were suspended in PBS and dead cells were stained with the Viakrome 808 Fixable Viability Dye (Beckman coulter). Cells were subsequently washed and suspended in staining buffer containing PBS, 1% FBS and 0.09% NaN3. Cells were first stained for surface markers, then fixed and permeabilized using the FOXP3/Transcription Factor Staining Buffer Set (ThermoFisher). After the permeabilization, cells were stained for intracellular cytokines and intracellular FOXP3. All the antibodies used are listed in the Key resources table: BV510 anti-mouse CD45 (BioLegend), Alexa Fluor 700 anti-mouse CD4 (BioLegend), Alexa Fluor 488 anti-mouse CD25 (BioLegend), PE-Cy7 anti-mouse LAG3 (BioLegend), APC-Cy7 anti-mouse CD49b (BioLegend), eFluor450 anti-mouse FOXP3 (Invitrogen), Alexa Fluor 647 anti-mouse IL-17A (BD Pharmingen), PerCP-Cy5 anti-mouse IFN-γ (BD Pharmingen), PE anti-mouse GM-CSF (BD Pharmingen), BV650 anti-mouse LPAM-1 (BD Pharmingen). Flow cytometry was performed using CytoFLEX LX and data were analyzed with FlowJo Software (v.10.8.1) using unstained and single-stained compensation beads as compensation controls. FMO as well as non-stimulated cells were used as a negative control. The gating strategy used in flow cytometry analysis to identify the different immune cell subsets is shown in Figure S9.

MOG-specific T cell recall assay

Draining lymph nodes (DLN) were isolated from EAE-immunized mice and smashed using a 70 μm cell strainer. Cells were washed in 1X PBS and counted. 2.5 x 10^5 cells for each condition were plated in a 96 multi-well plate (round bottom) and incubated at 37°C for 5 days in the presence of 10 μM of MOG_{35-55} peptide. Stimulation with Dynabeads Mouse T-Activator CD3/CD28 (ThermoFisher) was

used as a positive control. Unstimulated cells were included in the assay to assess background activation (negative control). After 5 days, cells were stimulated for 4h with Leukocytes Activation Cocktail with BD GolgiPlug following manufacturer's instruction (BD Biosciences) and stained for flow cytometry analysis. Briefly, cells were suspended in PBS and dead cells were stained with Fixable Viability Dye eFluor506 (ThermoFisher). Cells were subsequently washed and suspended in staining buffer containing PBS, 1% FBS and 0.09% NaN3 for the staining of cell surface markers. Cells were then fixed and permeabilized by using the BD Cytofix/Cytoperm kit, and finally stained for intracellular cytokines. The following antibodies were used: FITC anti-mouse CD3 (BD Bioscience), PerCP-Cy5.5 anti-mouse CD4 (BD Bioscience), APC-eFluor780 anti-mouse CD45 (Invitrogen), V450 anti-mouse IFN-γ (BD Bioscience), Alexa Fluor 647 anti-mouse IL-17A (BD Bioscience), PE anti-mouse GM-CSF (BD Bioscience). Flow cytometry was performed using FACSCanto III and data were analyzed with FlowJo Software (v.10.8.1) using unstained and single-stained compensation beads as compensation controls.

Dendritic cell generation and cell culture

Bone marrow dendritic cells (BMDC) were derived as previously described.[58] Briefly, bone marrow progenitors were cultured in RPMI-1640 medium supplemented with 10% FBS, 1% penicillin/streptomycin, 20 ng/mL granulocytes-macrophage colony-stimulating factor (GM-CSF, Miltenyi Biotec) and 10 ng/mL IL-4 (Miltenyi Biotec) to generate BMDC. On day 10, $5x10^4$/well BMDC were plated in 96-well plates and stimulated with lipopolysaccharide (LPS, 1 μg/mL, Sigma-Aldrich) with or without DCA and LCA (80 μM, alone or in combination) for 20h, and then washed and pulsed with 1 μg/mL of MOG_{35-55} peptide for additional 2 h. Mouse naive $CD4^+$ T cells from the spleen of 2D2 TCR^{MOG} transgenic mice were isolated using the mouse naive $CD4^+$ T cell isolation kit (Miltenyi Biotec). DCA/LCA pre-treated MOG-pulsed BMDC and naive $CD4^+$ T cells were co-cultured at 1:5 ratio. After 72h of co-culture, cells were harvested and analyzed by flow cytometry analysis upon stimulation and staining procedure as described above.

QUANTIFICATION AND STATISTICAL ANALYSIS

For human gut microbiota analysis, RNA-seq reads were first preprocessed to remove contaminants and trimmed. DESeq2 R package then removes low-expressing genes and performs normalization using a negative binomial model to estimate normalization factors prior to differential abundance analysis,[57] where FDR <0.1 were considered statistically significant. Species alpha diversity index based on Shannon index was calculated with vegan (https://cran.r-project.org/web/packages/vegan). Visualization was performed with ggplot2 and Krona. For human metabolomic analysis, data were generated upon Mann Whitney U test among the two experimental groups. Graphpad Prism version 8.0 (Graphpad Software) was used for statistical analysis. EAE clinical scores were analyzed with two-way ANOVA test followed by Bonferroni post-testing for multiple comparisons (cut-off value of 0.05). Disease incidence was evaluated using the Kaplan-Meier estimation, whereas statistical significance was evaluated by the log rank [Mantel-Cox] test. Other differences were estimated by two-tailed Student's t test or Mann Whitney U test or one-way ANOVA test. Multivariate analysis was performed by Spearman correlation coefficients and adjusted by FDR, using the ggstatsplot R package.[52] p values <0.05 were considered significant in all tests. All the statistical details of experiments including the statistical test used, n values and definition of center with dispersion measures (mean ± SD) can be found in the figure legends.